# Dynamics and Thermodynamics of Pd−PdO Phase Transitions: Effects of Pd Cluster Size and Kinetic Implications for Catalytic Methane Combustion

Ya-Huei (Cathy) Chin,[†] Mónica García-Diéguez, and Enrique Iglesia*

Department of Chemical and Biomolecular Engineering, University of California, Berkeley, California 94720, United States

S *Supporting Information*

ABSTRACT: Methane oxidation rates uncorrupted by nonchemical effects of transport, taken together with stoichiometric oxygen uptake (oxidation cycle) and evolution (decomposition cycle) data, are used to establish for the first time a set of conditions required for true thermodynamic equilibrium during metal-to-oxide interconversions in small Pd clusters (1.8−8.8 nm). These conditions allow us to assess the intrinsic thermodynamics of small Pd clusters and their catalytic effects in CH_4 oxidation. PdO decomposition in the absence of CH_4 deviates from equilibrium, as this step is limited by the nucleation of an oxygen vacancy ensemble on oxide domains. The nucleation bottleneck is removed by CH_4 during its catalytic sojourns, when CH_4 pressure and the related rates exceed a critical value, because CH_4 effectively removes the oxygen adatoms near an oxygen vacancy site via C−H bond activation on an oxygen−oxygen vacancy site pair that converts the O* adatom to a hydroxyl intermediate, which desorbs as H_2O in sequential steps. CH_4 oxidation turnovers promote the nucleation of oxygen vacancy ensembles at conditions that maintain the global oxygen equilibration, as confirmed from the absence of CH_4 oxidation rate hysteresis in both Pd oxidation and PdO decomposition cycles and from coincidence of rate and oxygen content profiles during Pd oxidation. A theoretical construction decoupling the inherent cluster size variance from cluster diameter effects shows marked effects of size on bulk phase transition. The bulk phase transition occurs at lower oxygen chemical potentials for the smaller clusters, which confirm their more negative Gibbs free energy for PdO formation than the large structures. The bulk phase transition converts O*−O* adatom sites to Pd^{2+}−O^{2-} ion pairs that are more effective for the kinetically relevant C−H bond activation in CH_4. These effects of size on the thermodynamics and reactivities of small clusters illustrated in this study are general and extend beyond the Pd−PdO system.
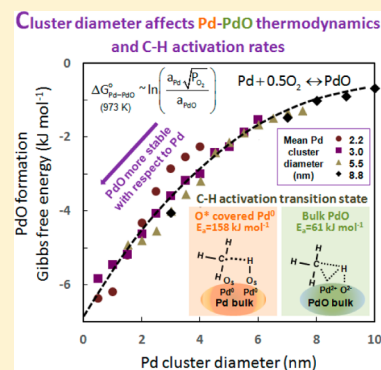
1. INTRODUCTION

A transition between the metal and oxide phases of Pd clusters occurs as oxygen atoms chemisorb on their surfaces and dissolve into their bulk as the oxygen chemical potential of reactant mixtures increases. These transitions can lead to reconstructions that change the shape and surface structure of Pd clusters.[1,2] As oxygen contents increase, the active sites for C−H bond activation in CH_4−O_2 reactions evolve from vicinal exposed Pd metal atoms (*−*), to chemisorbed oxygen site pairs (O*−O*), and ultimately to site pairs consisting of Pd^{2+} and lattice O^{2-} ions as bulk PdO structures form. These different active structures catalyze kinetically relevant C−H bond activation steps via distinct mechanisms: oxidative addition, homolytic C−H activation, and concerted oxidative addition−reductive deprotonation, which involve three-center $\{(H_3C\text{--}Pd\text{--}H)^‡\}$, radical-like $H_3C\bullet$ $\{(O^*\text{--}CH_3\bullet\text{--}^*OH)^‡\}$, and four-center $\{(H_3C^{\delta-}\text{--}Pd^{2+}\text{--}H^{\delta+}\text{--}O^{2-})^‡\}$ transition states, respectively.[3] These transition states differ in free energies and lead to very different activation barriers and pre-exponential factors, depending on the relative abundance of exposed oxygen and Pd atoms and on the chemical state of the Pd clusters.[3]

Previous studies have addressed phase transitions in Pd clusters and their consequences for CH_4 oxidation catalysis

using *in situ* (thermogravimetric analyses,[4] Raman spectra,[5] X-ray diffraction,[5] temperature-programmed adsorption−desorption[6]) and *ex situ* (transmission electron microscopy[7]) techniques. CH_4 oxidation rates and the effects of cluster size on turnover rates have been reported for metal[3] and oxide[8] clusters. The effects of cluster size and surface coordination on the thermodynamics and dynamics of Pd−PdO interconversions, however, remain controversial, as does their catalytic rates and the associated mechanistic interpretation during such phase transitions. Specifically, the bulk phase transitions and their catalytic consequences remain speculative in both mechanism and magnitude, at least in part, because of ubiquitous transport artifacts and of the uncertain value of the oxygen chemical potential that prevails at cluster surfaces during catalysis; these chemical potentials uniquely determine the thermodynamic and kinetic driving forces for phase transitions and for the elementary steps that mediate oxidation catalytic sequences. O_2 equilibration with chemisorbed and bulk oxygen phases is not always attained during CH_4−O_2

reactions on Pd, as evident from the ubiquitous observed hysteresis in catalytic reactivity upon Pd−PdO transformations brought forth by temperature cycling.[4,9]

A rigorous assessment of whether oxygen equilibration occurs and of the thermodynamic origins of the observed reactivity and structural transformations requires measurements of the oxygen content in clusters present in equilibrium with known oxygen chemical potentials (μ_{O_2}). This becomes possible only when such chemical potentials are the same throughout the gas phase and the surface and bulk of clusters ($\mu_{O_2,gas} = \mu_{O_2,surface} = \mu_{O_2,bulk}$); only in such cases, the (measurable) O_2 pressures in contact with the catalyst rigorously reflect oxygen chemical potentials. Bulk oxidation is often limited by the dissolution of chemisorbed oxygen (O_s^*; hereinafter subscript s denotes surface and * denotes a surface Pd atom) into the bulk phase,[10] leading to O contents that vary with cluster size and temperature, but as a consequence of dynamics instead of thermodynamics,[11,12] and to the coexistence of Pd and PdO metastable structures, which are precluded by the Gibbs phase rule at equilibrium. Such kinetic hurdles also corrupt PdO decomposition processes that are often limited by oxygen diffusion in PdO structures to form O_s^* species and/or by the recombinative desorption of chemisorbed O atoms (O_s^*), which are required to nucleate and grow a Pd metal phase. These metal-to-oxide phase transitions are ubiquitous in oxidation catalysis, but their most compelling, relevant, and explicit manifestations are evident in combustion reactions catalyzed by Pd−PdO systems because they occur at conditions of their relevant practice.

During catalysis, chemical potentials at surfaces reflect the kinetic coupling of steps that form (oxidation) and remove (reduction) O_s^* species; as a result, they depend on the oxidant and reductant concentrations and their respective activation rate constants.[13] Mechanistic inquiries to interpret this kinetic coupling during steady-state catalysis must be carried out under conditions of strict kinetic control, a significant challenge for very fast exothermic reactions, such as CH_4 oxidation [$\Delta H^\circ_{rxn} = -802$ kJ (mol CH_4)$^{-1}$], which invariably lead to bed and intrapellet gradients of temperature and concentrations. These ubiquitous artifacts tend to corrupt measurements of intrinsic rates, thus precluding unequivocal assessments of the kinetics, mechanism, and oxygen chemical potentials relevant for CH_4 combustion catalysis and for Pd−PdO interconversions.

Here, we report O_2 uptakes on Pd clusters (1.8−8.8 nm diameter) and the catalytic consequences of their O content for CH_4−O_2 reactions at oxygen chemical potentials prevalent during catalysis and responsible for Pd−PdO phase transitions. These data show that PdO decomposition is kinetically limited; thus, it represents an inappropriate descriptor of Pd−PdO−O_2 thermodynamics. These kinetic hurdles reflect O_s^* recombination bottlenecks, caused by the greater stability of O_s^* species as vicinal vacancies form, which prevents the nucleation of the Pd phase. These kinetic obstacles become less evident with increasing CH_4 pressures, apparently because C−H activation rates are higher near vacant sites, thus favoring the formation of Pd metal nuclei of critical size at PdO cluster surfaces.

In this study, the attainment of equilibrium was rigorously established by measuring intrinsic C−H bond activation rate constants without transport artifacts and under conditions for which the O content of Pd and turnover rates did not depend on path or sample history. The oxidation of Pd to PdO and the abrupt concurrent increase in CH_4 conversion rates occur at higher O_2 pressures (and oxygen chemical potentials) than those inferred from phase boundaries derived from PdO decomposition data and previously considered to represent the relevant thermodynamics. These O_2 pressures and the thermodynamic properties of the Pd−PdO system depend sensitively on cluster size, with Pd−PdO transitions occurring at lower O_2 pressures on smaller clusters, consistent with their stronger Pd−O bonds[14] and more negative Gibbs free energy for PdO formation. The rigorous thermodynamic origins of the measured oxygen uptakes and the intrinsic CH_4 oxidation turnover rates allow, for the first time, an accurate assessment and a mechanistic interpretation of Pd−PdO phase boundaries, of the strong effects of cluster size on their thermodynamic tendency for bulk oxidation, and of the concomitant effects of bulk oxidation on the reactivity of Pd clusters in CH_4 combustion catalysis.

2. EXPERIMENTAL METHODS

2.1. Catalyst Synthesis and Cluster Size Determination. γ-Al_2O_3 (Sasol North America Inc., Lot#C1643, 193 m² g^{-1}, 0.57 cm³ g^{-1} pore volume) was treated in flowing dry air (Praxair zero grade, 1.5 cm³ g^{-1} s^{-1}) at 1098 K for 5 h. Pd (0.6% wt. Pd) was deposited onto γ-Al_2O_3 by incipient wetness impregnation with aqueous $Pd(NO_3)_2$ (Aldrich CAS 380040, 99.999% purity, 10% wt. $Pd(NO_3)_2$ in 10% wt. HNO_3). The sample was treated in ambient stagnant air at 383 K for >8 h and divided into five portions, which were treated in flowing dry air (Praxair zero grade, 1.5 cm³ g^{-1} s^{-1}) at 623 K for 3 h and then heated (at 0.033 K s^{-1}) to 973, 1023, 1073, 1123, or 1173 K for 10 h to obtain Pd clusters with a broad range of metal dispersion. These five samples were subsequently heated to 923 K (at 0.033 K s^{-1}) in flowing 10 kPa H_2/He (Praxair UHP grade, 1.5 cm³ g^{-1} s^{-1}), held for 3 h, and cooled to ambient temperature in flowing He (Praxair UHP grade, 1.5 cm³ g^{-1} s^{-1}); samples were passivated by exposure to flowing 0.5 kPa O_2/He (Praxair Certified Standard grade, 0.5 cm³ g^{-1} s^{-1}) for 2 h before exposure to ambient air. Fractional metal dispersions were estimated from volumetric uptakes of strongly chemisorbed O_2 (1−30 kPa) at 313 K in a volumetric apparatus described in detail in the next section. Before uptake measurements, samples were treated at 773 K in flowing 10 kPa H_2/He (1.33 cm³ s^{-1}, Praxair UHP grade, 0.033 K s^{-1} heating rate) for 1 h and evacuated for 1 h and then cooled to 313 K in dynamic vacuum. After the O_2 uptakes, the samples were treated in dynamic vacuum at 313 K for 0.25 h and a second O_2 isotherm was measured. O_2 uptake measured in the second O_2 isotherm was negligible. The two resultant O_2 isotherms were extrapolated to zero O_2 pressure and their difference was used to estimate Pd dispersion, assuming an O:Pd stoichiometry of 1:1 (O/Pd$_s$ = 1). Cluster sizes were calculated from dispersion values by assuming hemispherical clusters and using the bulk Pd metal density (12.0 g cm^{-3}).[15]

Transmission electron microscopy (JEOL 1200 EX microscope) was used to determine the mean cluster diameter and size distributions of Pd clusters on the passivated samples (described above). The surface-averaged cluster diameters for these samples, $\langle d \rangle$, were calculated from the number of clusters (n_i) with a diameter of d_i, averaging over all clusters i, according to

$$\langle d \rangle = \frac{\sum n_i d_i^3}{\sum n_i d_i^2} \tag{1}$$

Scheme 1. Methane and Oxygen Activation Steps and the Types of Oxygen Species on the Surfaces of a Metallic Pd Cluster (a) and on the Surfaces and in the Bulk of a PdO Cluster (b) during CH$_4$–O$_2$ Reactions[a]
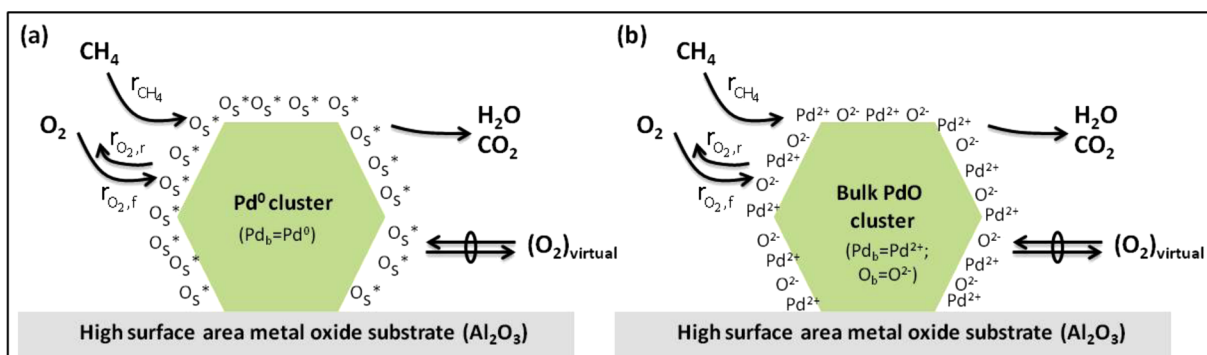
[a](O_s*: chemisorbed oxygen atom on Pd cluster surfaces, O_b: bulk oxygen atom, Pd_b: bulk Pd atom, Pd^{2+}–O^{2-}: Pd_{ox}–O_{ox} site pair on bulk PdO cluster surfaces, r_{CH_4}: forward rate of CH$_4$ conversion (Step 2 (2.a–2.d), Scheme 2), $r_{O_2,f}$: rate of O$_2$ dissociation (Step 1, Scheme 2), $r_{O_2,r}$: rate of O* recombination (Reverse of Step 1, Scheme 2), (O$_2$)$_{virtual}$: oxygen virtual pressure defined by eq 2b).
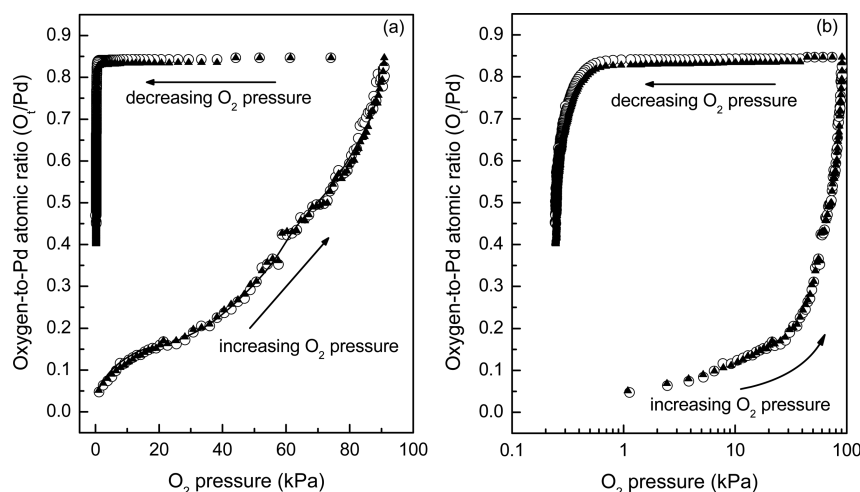

Figure 1. Oxygen content in Pd clusters (0.6% wt. Pd/Al$_2$O$_3$ catalyst, 8.8 nm mean cluster diameter) at 973 K, expressed as oxygen-to-Pd atomic ratio (O$_t$/Pd; O$_t$ = O$_s$* + O$_b$, Scheme 1) in linear (a) and logarithmic (b) scales, as a function of the prevalent O$_2$ pressure during uptake and decomposition cycles with dwell times of 3.6 ks (○) or 5.4 ks (▲).

2.2. Oxygen Uptake and Evolution Measurements. O contents were determined at 973 K by volumetric measurements of oxygen uptake or evolution as a function of O$_2$ pressure. The apparatus consists of a quartz tube with a fritted sample holder, a K-type thermocouple in contact with the outer tube wall, and a stainless steel dosing chamber (10–11 cm^3 reactor cell and 11.9 cm^3 dosing chamber; 5 × 10^{-4} mol of gas (STP) in the total chamber) with leak rates of <3 × 10^{-9} mol h^{-1} at ambient temperature and <6 × 10^{-9} mol h^{-1} at 973 K. Samples (~1 g) were treated at 773 K in flowing 10 kPa H$_2$/He (1.33 cm^3 s^{-1}, Praxair UHP grade, 0.033 K s^{-1} heating rate) for 1 h and evacuated for 1 h under dynamic vacuum using a turbomolecular (TMU 071 P, Pfeiffer) and a rotary vane (Varian DS 302) pump (1 × 10^{-6} Pa dynamic vacuum). Samples were heated in vacuum to 973 K (at 0.033 K s^{-1}) and held for 8 h before uptake and evolution measurements. O$_2$ uptakes were measured by increasing the O$_2$ pressure from 0.25 to 90 kPa by injecting O$_2$ pulses (Praxair UHP grade; 5–10 μmol O$_2$ per pulse) at 3.6 or 5.4 ks intervals. O$_2$ evolution was measured by decreasing the O$_2$ pressure stepwise at 3.6 or 5.4 ks intervals from 90 to 0.15 kPa in steps corresponding to the removal of 5–50 μmol of O$_2$ from the chamber. O$_2$ pressures

were measured using a dual-range pressure transducer (MKS Baratron, type D28B, 0–13.3 and 0–133.3 kPa pressure ranges; ±0.25% accuracy).

2.3. CH$_4$ Oxidation Rate Measurements. CH$_4$–O$_2$ turnover rates were measured at differential conditions (<5% CH$_4$ conversion) in a continuous flow packed-bed tubular reactor (quartz, 8.1 mm inner diameter) with plug-flow hydrodynamics. Pd/Al$_2$O$_3$ powders were diluted with SiO$_2$ [Davison Chemical, Chromatographic Silica Media, CAS no. 112926-00-8, 280 m^2 g^{-1}; treated in flowing dry air (Praxair, 99.99%, 0.8 cm^3 g^{-1} s^{-1}) at 0.083 K s^{-1} ramp to 1123 K and 5 h hold] at an intraparticle SiO$_2$-to-catalyst mass ratio of 100 and then pelleted to retain 106–250 μm aggregates. These aggregates were physically mixed with quartz (Fluka, acid purified, product number 84880; 106–250 μm diameter) at a quartz-to-aggregate mass ratio of 280. These dilution levels were sufficient to avoid temperature and concentration gradients at the heat loads of these experiments (<15 × 10^{-2} W cm^{-3}) for the 8 mm tubular reactors used here.[16]

Reactant concentrations were set by electronic flow meters (Porter 201) by mixing of O$_2$ (Praxair UHP grade) or 5% O$_2$/He (Praxair Certified Standard grade) with 25% CH$_4$/He

(Matheson Certified Plus grade) and He (Praxair UHP grade). O_2, CH_4, and CO_2 concentrations were measured by online gas chromatography (Agilent 3000A) using Poraplot Q or Mol Sieve 5A columns, each connected to a thermal conductivity detector. CO_2 and H_2O were the only products formed at all conditions: CO and H_2 were either not formed or under the detection limits (<10 ppm).

3. RESULTS AND DISCUSSION

3.1. O_2 Uptake and Evolution Measurements. Oxygen contents in Pd clusters are reported here as O-to-Pd atomic ratios (O_t/Pd), where O_t is the total oxygen atom uptake, given by the sum of the surface (O_s^*) and bulk (O_b) oxygen atoms (Scheme 1). The O_t/Pd ratios of 8.8 nm Pd clusters (0.6% wt. Pd/Al_2O_3) at 973 K are shown in Figure 1 as a function of O_2 pressure (0.25−91.0 kPa) during the uptake and evolution parts of the oxidation−reduction cycle using 3.6 or 5.4 ks dwell times at each O_2 pressure. Shorter dwell times (<3.6 ks) led to smaller O_t/Pd ratios (Figure S-1, Supporting Information) during oxygen uptake experiments (stepwise O_2 pressure increase), but longer times did not influence O_t/Pd ratios (3.6−5.4 ks), suggesting the absence of kinetic bottlenecks. These time-independent oxygen contents, by themselves, cannot unequivocally show that equilibrium was attained because dense impervious oxide layers may impede transport as they gradually form, leading to erroneous interpretations of the thermodynamic origins of these phenomena. Oxygen uptakes reached constant values at longer times during O_2 evolution (stepwise O_2 pressure decrease) than during O_2 uptake; O_t/Pd ratios continued to decrease even after 3.6 ks during evolution cycles (Figure 1 and Figure S-2, Supporting Information), indicating that kinetic bottlenecks were more significant during removal than uptake of oxygen atoms.

During oxygen uptake cycles, the O_t/Pd ratios at low O_2 pressures (<25 kPa O_2) were similar at 313 and 973 K. These ratios were also nearly independent of O_2 pressure (Figure S-3, 0.6% wt. Pd/Al_2O_3), consistent with Pd cluster surfaces saturated with a chemisorbed oxygen adatom (O_s^*). Extrapolating measured O_t/Pd ratios (Figure 1) to zero pressures gave similar O_t/Pd ratios at 313 and 973 K [e.g., $(O_t/Pd)_{P_{O_2}=0}$ = 0.113 (313 K) and 0.099 (973 K), where Pd denotes reducible Pd atoms]. These data indicate that Pd clusters retain their metallic bulk at these temperatures and low O_2 pressures, a conclusion supported by X-ray diffractograms. The extrapolated O_t/Pd ratio at 313 K (0.113) is used here to define the saturation uptake for this sample; this value corresponds to hemispherical clusters with a mean diameter of 8.8 nm.

O_t/Pd ratios increased monotonically (0.17 to 0.83) with increasing O_2 pressure (35 to 91 kPa) at 973 K. These values exceed the O_t/Pd ratios for an adsorbed monolayer (0.113; 0.6% wt. Pd/Al_2O_3, 8.8 nm mean cluster diameter). Thus, we conclude that O atoms dissolve into the cluster bulk at these higher O_2 pressures (>35 kPa) to form structures with O_t/Pd ratios (0.83) approaching those expected for stoichiometric PdO. This ratio is lower than unity because the high-temperature treatment required to form the large clusters may transform a portion of Pd to dispersed, irreducible oxides (e.g., Pd aluminate),[17] which remain invisible in the oxygen uptake experiments and largely unreactive toward methane activation.[8,18] A subsequent decrease in O_2 pressure from 91 to 0.6 kPa did not cause detectable O_2 evolution or changes in O_t/Pd ratios (0.84 ± 0.02). O_2 pressures below 0.6 kPa ultimately

led to O_2 evolution and to lower O_t/Pd ratios (Figure 1), consistent with the incipient decomposition of PdO. At each O_2 pressure, the O_t/Pd contents were much larger during oxygen evolution than uptake cycles (Figure 1), as also shown previously using temperature (instead of pressure) cycling.[4,6,9] Clearly, O_t/Pd ratios depend on the oxidation−decomposition path, making one or both uptake values at any given O_2 pressure of dubious thermodynamic relevance. At equilibrium, O contents must strictly reflect the prevalent oxygen chemical potential (in this case, the O_2 pressure), irrespective of path.

Longer dwell times (3.6 vs 5.4 ks) decreased O contents during PdO decomposition (Figure 1 and Figure S-2, Supporting Information), especially at low O_2 pressures (<0.4 kPa). These long transients reflect slow recombinative desorption of lattice oxygens (O_{ox}) from PdO crystallites, a step that requires the formation of unstable vacancy pairs ($2O_{ox} \rightarrow O_2(g)+2\square$, where $\square$ denotes a lattice oxygen vacancy). The energy required to incipiently evolve O_2 from stoichiometric PdO has been reported to be 202 kJ mol^{-1} on 67 nm PdO clusters and 349 kJ mol^{-1} on 1 nm PdO clusters.[14] This value is expected to be even higher as the oxygen content decreases below its stoichiometric value as PdO decomposition proceeds. Indeed, the energy required to form additional oxygen vacancies increases markedly as the number of vacancies increases, as shown by density functional theory (DFT) calculations on the bulk Cu−CeO_2 system, for which the removal of O atoms from oxygen-deficient Cu−CeO_{2-x} structures was much more endothermic (by 130 kJ mol^{-1}) than for the removal of the first O atom in stoichiometric Cu−CeO_2.[19] The diffusion of oxygen from the bulk to the surface of PdO can also limit decomposition rates because activation barriers for oxygen diffusion are higher in PdO than in Pd single crystals (111−116 kJ mol^{-1} for PdO vs 60−85 kJ mol^{-1} for Pd).[20] These transport bottlenecks may also prevent equilibration during PdO decomposition cycles. The nucleation of a Pd metal phase involves the formation of ensembles of oxygen vacancies via desorption of oxygen (O_{ox}) species, which become more strongly bound near such ensembles, thus inhibiting the coalescence of reduced centers into nuclei of critical size. Such local stabilization of lattice oxygen (O_{ox}), together with the activated nature of oxygen diffusion from the PdO bulk, poses formidable kinetic hurdles to the attainment of equilibrium during PdO decomposition and allows PdO to exist at oxygen chemical potentials well below those prescribed by the Gibbs free energy for its transformation to Pd metal.

These significant kinetic hurdles and the nonequilibrium nature of PdO decomposition cast doubts about the prevailing use of PdO decomposition processes to determine Pd−PdO thermodynamics.[21−25] Our evidence for the kinetic nature of PdO decomposition steps remains silent, however, about whether O_t/Pd ratios measured during oxidation cycles also reflect the dynamics instead of the thermodynamics of PdO oxidation because of slow O_2 dissociation or O* diffusion within Pd metal clusters. Even if oxygen equilibration was attained during uptake measurements, it may not be achieved during steady-state CH_4−O_2 reactions because the scavenging of O_s^* species by CH_4 coreactants can prevent $O_2(g)$−O_s^* equilibration; in doing so, oxygen chemical potentials at cluster surfaces can become lower than in the contacting gas phase. In what follows, we show that equilibration is indeed attained during steady-state catalysis, that the presence of CH_4 facilitates the nucleation of Pd metal domains (without disturbing the O_2−O_s^* equilibration), and that the O_t/Pd ratios measured

during uptake cycles in the absence of CH_4 accurately reflect the thermodynamics of Pd−PdO transformations.

3.2. O_2 Adsorption−Desorption Equilibration during Steady-State CH_4−O_2 Catalysis.

In this section, we examine the conditions required for equilibration among gaseous, surface, and bulk forms of oxygen during contact between Pd clusters and $O_2(g)$ in the presence or absence of CH_4 coreactants.

During catalysis, the chemical potential prevalent at surfaces is imposed by a virtual pressure of oxygen $[(O_2)_{virtual}]$, defined as the (hypothetical) O_2 pressure that would lead to the coverages of chemisorbed oxygen (O_s^*) present during steady-state catalysis if adsorption−desorption equilibrium was to prevail

$$(O_2)_{virtual} + 2^* \overset{K_{O_2}}{\longleftrightarrow} 2O_s^* \tag{2a}$$

$$\frac{(O_s^*)}{(^*)} = \sqrt{K_{O_2}(O_2)_{virtual}} \tag{2b}$$

Here, K_{O_2} is the equilibrium constant for O_2 dissociative adsorption (Step 1 in Scheme 2), and * denotes a surface Pd

Scheme 2. Elementary Steps for O_2 Dissociation and C−H Bond Activation during CH_4−O_2 Reactions on Supported Pd and PdO Clusters[a]

Elementary Step		Kinetic and thermodynamic constant
1	$(O_2) + 2^* \rightleftarrows 2O_s^*$	$k_{O_2,f}$; $k_{O_2,r}$; K_{O_2}
2.a	$CH_4 + ^* + ^* \rightarrow CH_3^* + H^*$	$k_{CH_4,^*-^*}$
2.b	$CH_4 + O_s^* + ^* \rightarrow CH_3^* + OH^*$	$k_{CH_4,O_s^*-^*}$
2.c	$CH_4 + O_s^* + O_s^* \rightarrow CH_3O^* + OH^*$	$k_{CH_4,O_s^*-O_s^*}$
2.d	$CH_4 + Pd^{2+} + O^{2-} \rightarrow CH_3Pd^{2+} + HO^{2-}$	$k_{CH_4,Pd^{2+}-O^{2-}}$

[a]* refers to an unoccupied Pd surface atom; → denotes an irreversible step; ⇄ denotes a reversible step; $k_{O_2,f}$: forward rate constant for O_2 dissociation; $k_{O_2,r}$: reverse rate constant for O_2 dissociation; $k_{CH_4,i}$: forward rate constant for CH_4 activation, where subscript i denotes the identity of active site pairs, $i = ^*-^*$, $O_s^*-^*$, $O_s^*-O_s^*$, or $Pd^{2+}-O^{2-}$; K_{O_2}: equilibrium constant for oxygen dissociation.

atom. The value of $(O_2)_{virtual}$ represents a rigorous (and often measurable) proxy for the prevalent oxygen chemical potential and all its kinetic and thermodynamic consequences, as shown from nonequilibrium thermodynamic formalisms of chemical kinetics.[26] The concept of virtual pressures has been used to rigorously describe the prevalent chemical potentials of oxygen at catalytic sites in CH_4,[13] C_2H_6,[27] and NO[28−30] oxidation, of nitrogen in NH_3 decomposition,[31] and of hydrogen in dehydrogenation catalysis.[32,33]

The $(O_s^*)/(^*)$ ratio and the value of $(O_2)_{virtual}$ (eq 2b) during steady-state catalysis reflect the kinetic coupling of elementary steps that form and consume O_s^* species

$$r_{O_2,f} = r_{O_2,r} + 2r_{CH_4} \tag{3}$$

Here, $r_{O_2,f}$, $r_{O_2,r}$, and r_{CH_4} represent the rates of O_2 dissociation (forward direction of Step 1, Scheme 2), O_s^* recombination (reverse direction of Step 1, Scheme 2), and CH_4 activation (irreversible Steps 2.a−2.d, Scheme 2). CH_4 activation may proceed on metal−metal ($^*-^*$; Step 2.a), oxygen−metal ($O_s^*-^*$; Step 2.b), or oxygen−oxygen ($O_s^*-O_s^*$; Step 2.c) site pairs on metal surfaces (Pd,[16] Pt[13]) via kinetically distinct

paths that involve oxidative addition, oxidative addition−hydrogen abstraction, or hydrogen abstraction steps, respectively; C−H bond activation occurs on $Pd^{2+}-O^{2-}$ ion pairs (Step 2.d) at PdO surfaces via the oxidative addition−reductive deprotonation step.[3] Thus, the r_{CH_4} term in eq 3 reflects the contributions from each of these paths and depends on their respective C−H activation rate constants ($k_{CH_4,i}$, subscript i denotes the identity of the active site pair, i.e., $^*-^*$, $O_s^*-^*$, $O_s^*-O_s^*$, or $Pd^{2+}-O^{2-}$, in Steps 2.a−2.d, Scheme 2). The $(O_s^*)/(^*)$ ratios and the corresponding $(O_2)_{virtual}$ values are then given by

$$\frac{(O_s^*)}{(^*)} = \sqrt{K_{O_2}(O_2)_{virtual}}$$

$$= f(k_{O_2,f}, k_{O_2,r}, k_{CH_4,i}, P_{CH_4}, P_{O_2}) \tag{4}$$

where f is a function of the rate constants for O_2 dissociation ($k_{O_2,f}$, forward of Step 1), O_s^* recombination ($k_{O_2,r}$, reverse of Step 1), and CH_4 activation ($k_{CH_4,i}$, Steps 2.a-2.d), as defined in Scheme 2, and of the prevalent CH_4 (P_{CH_4}) and O_2 (P_{O_2}) pressures.

The functional form of f in eq 4 depends on the nature of the site pairs involved in the C−H bond activation step ($^*-^*$, $O_s^*-^*$, $O_s^*-O_s^*$, or $Pd^{2+}-O^{2-}$).[3,16] When O_s^* recombination (reverse of Step 1, Scheme 2) occurs much faster than CH_4 activation (Steps 2a−2d, Scheme 2) ($r_{O_2,r} \gg r_{CH_4}$), the $(O_s^*)/(^*)$ ratios (eq 4) are not affected by CH_4 pressure because CH_4 reactions scavenge O_s^* slowly. As a result, such reactions do not perturb the $O_2(g)-O_s^*$ equilibrium (Step 1) or the prevalent oxygen chemical potentials. $(O_2)_{virtual}$ becomes equal to the contacting $O_2(g)$ pressure, and by definition oxygen chemical potentials at Pd cluster surfaces equal those of $O_2(g)$ during catalysis. O_s^* coverages and the thermodynamic tendency for phase transitions then depend solely on the prevalent O_2 pressures and are not influenced by the presence or pressure of CH_4. The oxygen contents measured in the absence of CH_4 coreactants (e.g., as reported in Section 3.1) would then rigorously reflect those actually present during steady-state CH_4 oxidation catalysis.

We examine next the extent of $O_2(g)-O_s^*$ equilibration during CH_4-O_2 reactions at 973 K and 8−82 kPa O_2. Figure 2 shows the measured first-order rate coefficients for CH_4 activation $[r_{CH_4}(CH_4)^{-1}$, defined as the turnover rate divided by CH_4 pressure] on Pd clusters (8.8 nm, 0.6% wt. Pd/Al_2O_3) as a function of O_2 pressure during cycles of increasing or decreasing O_2 pressure. At low O_2 pressures (<1.6 kPa O_2), these rate coefficients reflect the C−H activation rate constants (k_{CH_4,O^*-O^*}) on vicinal oxygen atom pairs ($O_s^*-O_s^*$; Step 2.c, Scheme 2), which are present at near saturation O^* coverages on Pd cluster surfaces.[3,16] At each O_2 pressure, the Pd bulk remains metallic with or without CH_4 coreactants, but their surfaces are saturated with chemisorbed oxygen ($O_s/Pd_s = 1.06$ at 873 K;[16] $O_s/Pd_s = 0.87$ at 973 K, Section 3.1; Pd_s refers to the surface Pd atom).[3,16] At these high temperatures and low conversions, CO_2 and H_2O do not influence reaction rates,[3] a conclusion confirmed here by the strict linear dependence of rates on CH_4 pressure. Extrapolation of the O_t/Pd ratios measured at low O_2 pressures (<35 kPa) to zero O_2 pressure gives similar O_t/Pd ratios at each temperature (313−973 K) (Supporting Information, Section 2, Figure S-3 for O_2
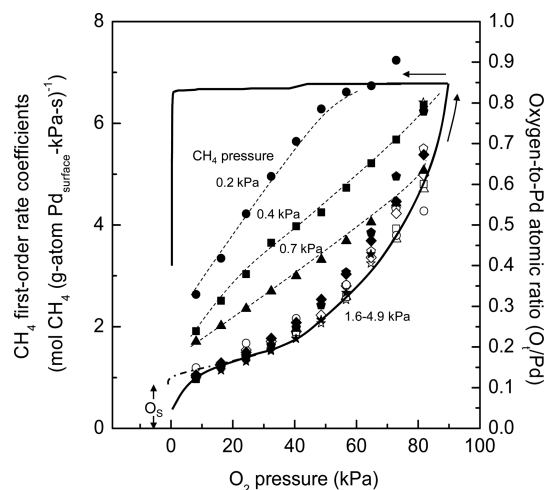
Figure 2. First-order rate coefficients for CH_4 oxidation $(r_{CH_4}(CH_4)^{-1})$ during stepwise increase (open symbols) and decrease (solid symbols) in O_2 pressure cycles with CH_4–O_2 mixtures on 0.6% wt. Pd/Al_2O_3 (8.8 nm mean Pd cluster diameter) at 973 K and 0.2 kPa ($\bigcirc$,$\bullet$), 0.4 kPa ($\square$,$\blacksquare$), 0.7 kPa ($\triangle$,$\blacktriangle$), 1.6 kPa ($\diamondsuit$,$\blacklozenge$), 2.4 kPa ($\triangleleft$,$\blacktriangleleft$), and 4.9 kPa ($\star$,$\bigstar$) CH_4. The solid lines denote the oxygen-to-Pd atomic ratios (O_t/Pd) during uptake and evolution in the absence of CH_4 (from Figure 1) ($\rightarrow$ denotes the direction of either increasing or decreasing O_2 pressure;. $\cdots\cdots$ denotes O_t/Pd ratios during contact with 10–35 kPa O_2 in the absence of CH_4 at 313 K). CH_4–O_2 rates were measured at 6.51×10^8 cm^3 (s mol $Pd_{surface}$)$^{-1}$.

Figure 3. First-order rate coefficients for CH_4 oxidation $(r_{CH_4}(CH_4)^{-1})$ during stepwise increase (open symbols) and decrease (solid symbols) in O_2 pressure with CH_4–O_2 mixtures [1.6 kPa ($\diamondsuit$,$\blacklozenge$), 2.4 kPa ($\triangleleft$,$\blacktriangleleft$), and 4.9 kPa ($\bigcirc$,$\bullet$) CH_4] on 0.6% wt. Pd/Al_2O_3 (8.8 nm mean Pd cluster diameter) at 973 K. CH_4–O_2 rates were measured at 6.51×10^8 cm^3 (s mol $Pd_{surface}$)$^{-1}$. The oxygen-to-Pd atomic ratios (O_t/Pd) during stepwise increase in O_2 pressure in the absence of CH_4 (from Figure 1) are also plotted here for comparison ($\square$).

adsorption isotherms on 3.0 and 8.8 nm Pd clusters at 313 and 973 K). At these O_2 pressures (e.g., 0.2–0.6 kPa) and 873 K, the rates of $^{16}O^{18}O$ isotopologue formation were similar for CH_4–$^{16}O_2$–$^{18}O_2$ (4.86 kPa CH_4) and $^{16}O_2$–$^{18}O_2$ mixtures; therefore, O_s* coverages, which determine isotopic exchange rates, are not affected by reactions with CH_4, and O_2 dissociation steps remain quasi-equilibrated during CH_4–O_2 reactions $\{(O_2)_{virtual} = O_2(g)\}$.[16] These data contrast those reported previously on Pt clusters, for which C–H bond activation steps, instead of O_s* desorption, represent the faster O_s* removal pathway during CH_4[13] and C_2H_6[27] oxidation at coverages below saturation; as a result, the $(O_2)_{virtual}$ on these Pt-based catalysts depends on CH_4 pressure, through the kinetically relevant coupling of C–H and O_2 activation steps.

First-order rate coefficients for CH_4 oxidation (973 K) on Pd clusters (8.8 nm, 0.6% wt. Pd/Al_2O_3) increased slightly between 8 and 35 kPa O_2 and then sharply above 35 kPa O_2 (Figures 2 and 3). O_s* species, which prevail on Pd metal surfaces at lower O_2 pressures (8–35 kPa), act as basic moieties that abstract H atoms from CH_4, as in the case of C–H activation in alkanes (CH_4[13] and C_2H_6[27] on Pt, CH_4 on Pd[3,16]) and alkenes (C_3H_6 and C_4H_8 on O_s*-covered Pd(100)[34]) on transition metal catalysts (Pt,[13,27] Pd[3,16,34]). As O_2 pressures increase and O_s* monolayers densify, O_s* species bind more weakly [binding energy decreases by 39 kJ mol^{-1} between 0.25 and 0.5 ML O* on Pd(111)[35]] and become more basic, thus acting as stronger electron donors during H abstraction.[3] Rate coefficients increased sharply at a critical O_2 pressure (>35 kPa O_2 for 8.8 nm clusters, 973 K, Figure 3), which coincides with that leading to O contents higher than monolayer values; at these pressures, O atoms dissolve into the cluster bulk, and Pd^{2+} ions become exposed at surfaces as PdO incipiently forms. This is likely to occur first on the smaller clusters present within
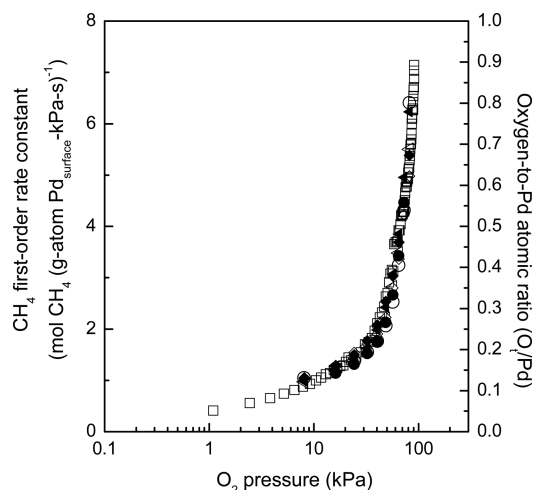
each sample as O_2 pressure increases because of their greater thermodynamic tendency toward bulk oxidation (Sec. 3.4).

The rate constants for C–H bond activation increased with increasing oxygen chemical potential, as more Pd clusters within each sample oxidized to PdO. CH_4 molecules can access both O atoms and metal centers in a concerted manner on PdO surfaces, making it possible for C–H bonds to cleave more effectively via oxidative addition–reductive deprotonation steps (Step 2.d, Scheme 2).[3] These steps are mediated by four-center $(HC_3^{\delta-}-Pd^{2+}-O^{2-}-H^{\delta+})^{\ddagger}$ transition states stabilized by $HC_3^{\delta-}-Pd^{2+}$, $Pd^{2+}-H^{\delta+}$, $O^{2-}-H^{\delta+}$, and $HC_3^{\delta-}-H^{\delta+}$ interactions, which are more stable than the radical-like $(O^*--CH_3\bullet--^*OH)^{\ddagger}$ transition states involved when C–H bonds are activated on O*-saturated Pd metal surfaces, in which CH_3 groups interact weakly with the O*–O* site pair and with the leaving H atom.[3,16] C–H bond activation barriers are much smaller on PdO than on O*-saturated Pd surfaces [measured: 61 vs 158 kJ mol^{-1}; DFT-derived C–H activation barriers of 62 vs 145 kJ mol^{-1} on PdO(101) vs O*-saturated Pd(111)], and the respective measured rate constants are much larger on PdO than O*-saturated Pd surfaces [measured 12.9 vs 0.53 mol CH_4 (g-atom $Pd_{surface}$-s-kPa)$^{-1}$ at 873 K, on 21.3 nm Pd clusters].[3] Similar routes and the involvement of Pd^{2+} and O^{2-} centers have been reported for the activation of larger alkanes (C_3H_8 and C_4H_{10}) on PdO(101) surfaces, during which C–H activation transition states interact with the surfaces via σ-complexes and dative bonds.[36]

During increasing O_2 pressure cycles, C–H activation rate coefficients $[r_{CH_4}(CH_4)^{-1}]$ at each O_2 pressure were not affected by CH_4 pressure (0.2–4.9 kPa, Figures 2 and 3). These data indicate that the C–H bond activation remains the sole kinetically relevant step and that the number of accessible Pd^{2+}–O^{2-} sites and the O-content of the clusters are not affected by scavenging of O atoms by CH_4 on both metal and oxide surfaces and during the bulk phase transition. Therefore, O_2 dissociation steps must be at equilibrium during CH_4–O_2 reactions $(r_{CH_4} \ll r_{O_2,r}$ and $r_{O_2,f} \approx r_{O_2,r}$; eq 3), and the prevalent

O_2 pressures establish the oxygen chemical potential and the O-content in Pd clusters during steady-state catalysis; these O_t/Pd ratios must then be identical to those measured during contact of Pd clusters with $O_2(g)$ at the same O_2 pressure and in the absence of CH_4 (Figures 2 and 3).

Measured rate coefficients (k_{CH_4}) during increasing O_2 pressure cycles are single-valued functions (g) of the O content (expressed as O_t/Pd) over the entire range of O_2 pressure

$$\frac{r_{CH_4}}{(CH_4)} = k_{CH_4} = g\left(\frac{O_t}{Pd}\right) \tag{5}$$

These rate coefficients increase with increasing oxygen content, apparently in response to Pd−PdO phase transitions. Throughout this transformation, C−H bond activation remains the sole kinetically relevant step, as shown from the effects of CH_4 pressure on rates and from DFT treatments of elementary steps on O*-covered Pd metal and oxide surfaces.[3] Measured rate coefficients (k_{CH_4}) and O contents (O_t/Pd) both reflect their ensemble averages over clusters that are distributed in size within each sample. The effects of size on their oxidation tendencies and the effects of oxidation state on reactivities are discussed in Sections 3.4 and 3.5, respectively.

C−H activation rate coefficients decreased monotonically with decreasing O_2 pressure (from 82 kPa O_2; Figure 2; solid symbols) as O atoms desorbed from PdO and Pd metal ensembles incipiently formed. These effects became stronger as CH_4 pressure increased, causing rate coefficients to become sensitive to CH_4 pressure during PdO decomposition but not during Pd oxidation cycles (Figure 2; symbols: solid for decomposition, open for oxidation). For example, the rate coefficients on PdO remained constant as O_2 pressure decreased from 82 to 60 kPa [6.7 mol CH_4 (g-atom $Pd_{surface}$-s-kPa)$^{-1}$; 0.2 kPa CH_4 (Figure 2; ●)]. At lower O_2 pressures (<60 kPa), these coefficients decreased with O_2 pressure but remained much larger than during uptake cycles at all O_2 pressures {e.g., k_{CH_4} = 2.6 (●) vs 1.2 (○) mol CH_4 (g-atom $Pd_{surface}$-s-kPa)$^{-1}$ at 0.2 kPa CH_4 and 8 kPa O_2}. Such hysteresis behavior became less evident at higher CH_4 pressures and was no longer detectable above 1.6 kPa CH_4, for which rate coefficients were the same during Pd oxidation and PdO decomposition cycles (Figures 2 and 3). At CH_4 pressures above 1.6 kPa, O_2 pressure effects on rate coefficients were independent of path and of CH_4 pressure, consistent with the attainment of chemical equilibrium between $O_2(g)$ and all oxygen-containing species present during CH_4 oxidation catalysis.

These data indicate that CH_4 molecules are required for Pd−PdO equilibration during PdO decomposition but not during Pd oxidation cycles. A plausible mechanistic interpretation for such phenomena involves the formation of Pd^0 nuclei, which require O* recombination events that form oxygen vacancies during PdO decomposition. The formation of these vacancies leads to stronger vicinal Pd−O bonds, thus inhibiting the growth of metal nuclei to their critical size for incipient PdO decomposition. As a result, subsequent O atom desorption and PdO decomposition occur only when oxygen chemical potentials are much lower than predicted from thermodynamics. In contrast, the presence of an oxygen vacancy causes a local increase in CH_4 activation rates because Pd centers stabilize the CH_3 fragments at C−H activation transition states,[16] as also reported on Pt surfaces partially covered with

O*.[13] Such processes favor the removal of oxygen (via reaction with CH_4) near oxygen vacancies, thus promoting the formation of vacancy ensembles and the growth of Pd^0 nuclei to critical size. The preferential activation of CH_4 near oxygen vacancies avoids the metastable character of PdO that is evident without reductants, even though CH_4 does not influence the prevalent oxygen chemical potentials that determine Pd−PdO transitions. The hysteresis behavior of both reactivity (at <1.6 kPa CH_4) and O content (during contact with $O_2(g)$) during PdO decomposition cycles (Figure 2) indicates that reactivity and O contents are higher during PdO decomposition than for surface and bulk phases in equilibrium with prevalent O_2 pressures, making the O content during decomposition an inaccurate measure of the Gibbs free energy for Pd−PdO transformations. In contrast, the identical rate coefficient values during oxidation and decomposition cycles for CH_4 pressures above 1.6 kPa at each O_2 pressure (Figure 3) confirm that the chemical state of Pd clusters is independent of path and history, and thus oxygen species among gaseous, surface, and bulk phases have attained equilibration, making such data of rigorous thermodynamic origins.

3.3. O_2−Pd−PdO Thermodynamic Phase Diagrams. The relevant thermodynamic evidence, derived here from changes in rate coefficients and in O_t/Pd values with oxygen chemical potentials, is used next to assess Pd−PdO phase boundaries for clusters with 1.8−8.8 nm in mean diameters. In doing so, we also report (in Section 3.4), seemingly for the first time, the effects of Pd cluster size on their *thermodynamic* oxidation tendencies, uncorrupted by the dynamics of nucleation and growth. The single-valued relations between O_t/Pd ratios and first-order CH_4 rate coefficients at all O_2 pressures (function g in eq 5; Figure 3) during Pd oxidation make first-order CH_4 rate coefficients rigorous proxies for oxygen contents, thus allowing the detection of bulk oxidation during CH_4 oxidation catalysis at oxygen chemical potentials (μ_{O_2}) that are identical among the gas phase, the adsorbed phase, and the bulk of the PdO_x clusters ($\mu_{O_2,gas} = \mu_{O_2,surface} = \mu_{O_2,bulk}$).

The onset of bulk oxidation occurs at an oxygen chemical potential (given by the prevalent O_2 pressure, Section 3.2) that causes the incipient dissolution of O_s^* atoms into the bulk and Pd clusters covered with O_s^* to undergo bulk phase transitions. This chemical potential is defined here as the O_2 pressure at which the rate coefficients reach 10% of their increase as Pd clusters saturated with chemisorbed oxygen convert to stoichiometric PdO clusters

$$\frac{(r_{CH_4}(CH_4)^{-1})_{PdO_j} - (r_{CH_4}(CH_4)^{-1})_{O^*/Pd}}{(r_{CH_4}(CH_4)^{-1})_{PdO} - (r_{CH_4}(CH_4)^{-1})_{O^*/Pd}} = 0.1 \tag{6}$$

Here, $(r_{CH_4}(CH_4)^{-1})_{PdO_j}$ denotes the rate coefficient at a specific mean oxygen content j ($j < 1$) for the clusters, averaging over all clusters of different sizes present in a given sample. The value that satisfies eq 6 defines the onset pressure, and the terms with subscripts O*/Pd and PdO denote rate coefficient values for O*-covered Pd and bulk PdO, respectively. For 8.8 nm Pd clusters, this onset occurs for a $(r_{CH_4}(CH_4)^{-1})_{PdO_j}$ value of 1.9 mol CH_4 (g-atom $Pd_{surface}$-kPa-s)$^{-1}$ at an onset pressure of 35 kPa O_2 at 973 K (Figure 3). The onset O_2 pressure for PdO decomposition is similarly defined as the O_2 pressure required for rate coefficients
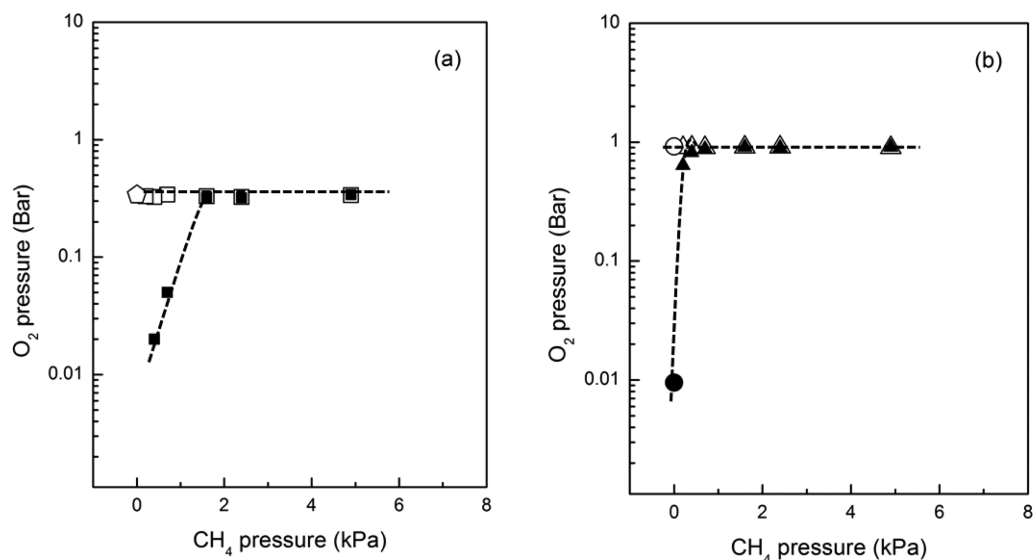
Figure 4. (a) O_2 pressures required for the onset of Pd oxidation ($\square$,$\hexagon$) or PdO decomposition ($\blacksquare$), plotted as a function of the contacting CH_4 pressure at 973 K. (b) O_2 pressures required to reach an O_t/Pd ratio of 0.85 during Pd oxidation ($\triangle$,$\bigcirc$) or PdO decomposition ($\blacktriangle$,$\bullet$), plotted as a function of the contacting CH_4 pressure at 973 K. Values in the absence of CH_4 ($\bigcirc$, $\hexagon$, $\bullet$) were obtained during O_2 uptake-evolution experiments in Figure 1 (0.6% wt. Pd/Al_2O_3, 8.8 nm mean Pd cluster diameter; dashed lines are drawn as a guide).

$[(r_{CH_4}(CH_4)^{-1})_{PdO}$; Figure 1] to decrease from the value corresponds to PdO to one that satisfies eq 6. This definition (eq 6), based on changes in rate coefficient and the related mean oxygen content, corresponds to the bulk oxidation of the majority of the clusters in each sample because smaller clusters oxidize at lower oxygen chemical potentials than larger clusters (as shown later in Section 3.4), and as a result of their size and concomitantly smaller number of Pd atoms per cluster, their oxidation requires fewer oxygen atoms. It is estimated that ~75% of all clusters in a sample are oxidized for the samples with 1.8 and 2.2 nm mean diameters, and the value becomes ~50% for those with 3.0 and 8.8 nm mean diameters. These estimations are derived from a theoretical construct that isolates cluster size effects from those caused by size variance within a catalyst sample, by accounting for their size distributions, as described in Section 3.4.

These onset pressures are shown as a function of CH_4 pressure (0−4.9 kPa) in Figure 4a for Pd oxidation and PdO decomposition. The onset O_2 pressures were also determined from O_2 uptakes (Figure 1, Section 3.1); they are similarly defined, but using the O contents as Pd clusters transforms from O*-covered metal to bulk oxide. In addition to these onset O_2 pressures, O_2 pressures required to increase the oxygen content (O_t/Pd) to a larger value of 0.85 were also determined with similar definitions from rate coefficient and oxygen uptake data (i.e., replacing the 0.1 with 0.85 in eq 6) and shown in Figure 4b as a function of CH_4 pressure (0−4.9 kPa). Onset O_2 pressures for bulk oxidation determined from O uptakes (Figure 4; $\hexagon$) are similar to those derived from C−H activation rate coefficients as O_2 pressure increases ($\square$, at all CH_4 pressures) or decreases ($\blacksquare$; for CH_4 pressures above 1.6 kPa), which occurred at 0.35 bar O_2 (at 973 K; 8.8 nm clusters). In contrast, the O_2 pressures required for PdO decomposition (8.8 nm) were much lower without CH_4; the O_t/Pd ratio did not reach 0.1 (defined in eq 6) but decreased slightly to 0.85 (Figure 4b, $\bullet$) for O_2 pressures as low as 0.0095 bar.

The onset O_2 pressures for Pd−PdO transitions determined from O contents and rate data are compared next with those reported previously for Pd−PdO phase transitions at conditions presumed to attain thermodynamic equilibrium[4−6,21−23,37−41] on Pd(111) extended surfaces,[37,38] supported clusters,[4,5,39,40] and bulk powders[21,22,41] over a broad range of temperature (500−1145 K) and O_2 pressure (1.3×10^{-12}−1.0 bar). These results were obtained from oxidation or decomposition during temperature ramps,[4,5,40] in situ Raman and X-ray diffraction,[5] gravimetric analysis,[21,22,39] scanning tunneling microscopy,[37] low-energy electron diffraction,[37] and X-ray photoelectron spectroscopy.[38] Such onset pressures are shown in the Supporting Information (Figure S-4 for PdO decomposition and Figure S-5 for Pd oxidation).

The O_2 pressure for incipient bulk oxidation (defined in eq 6) reflects the mean Gibbs free energy for PdO formation from Pd^0 (ΔG^o_{Pd-PdO}, per g-atom Pd, 1 bar reference state) for all clusters distributed in sizes within a sample

$$nPd + 0.5(n)O_2(g) \overset{K_{O_2}}{\longleftrightarrow} nPdO \tag{7a}$$

$$\Delta G^{\circ}_{Pd-PdO} = -RT \ln\left(\frac{a_{PdO}}{a_{Pd}P_{O_2}^{0.5}}\right) \tag{7b}$$

n is the mean number of Pd atoms in a cluster; and K_{O_2} is the equilibrium constant for Pd and PdO interconversion. Here, thermodynamic activities are unity for PdO and Pd phases (a_{PdO} and a_{Pd}) and P_{O_2} is the O_2 pressure (in bar). The onset pressures for Pd to PdO phase transition and the related Gibbs free energy for PdO formation must be independent of the intermediates or path involved in the transformation of Pd^0 clusters to O*-saturated Pd metal clusters and ultimately to bulk PdO. Thus, Gibbs free energies derived from measured onset pressures as Pd clusters evolve from metallic, to O* covered, and then to PdO clusters reflect the thermodynamics of Pd to PdO transformations (described in Supporting Information, Section 4). These free energies are shown together with previously reported values[4−6,21−23,37−40,39] from
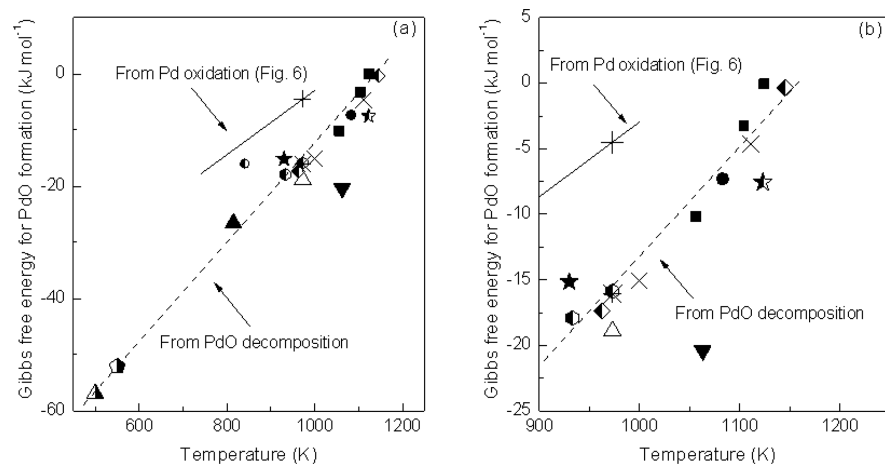
Figure 5. Gibbs free energy for PdO formation ($\Delta G^{\circ}_{Pd-PdO}$, per g-atom of Pd, eq 7) determined from PdO decomposition (8.8 nm mean Pd cluster diameter) in CH_4-O_2 mixtures (+; 4.85 kPa CH_4), oxygen uptake and evolution measurements (in O_2, Δ) in the present work, and those reported in the literature determined by PdO decomposition in O_2 (polycrystalline Pd: ■,[21] half-filled diamond,[22] half-filled star,[40] half-filled pentagon,[41] ∗;[23] supported Pd clusters: ●,[39] ×,[25] ▼,[5] half-filled hexagon,[4] and ★;[6] single crystal surfaces: ▲ [Pd(111)],[38] △ [Pd(100)][43]) and in CH_4-O_2 mixtures (supported Pd clusters: ◐[4]); - - - denotes the Pd–PdO phase boundary determined from regression analysis of the literature PdO decomposition data shown in this figure; — denotes the Pd–PdO phase boundary determined from the literature Pd oxidation data (Figure 6); (b) is the enlarged plot of the high-temperature region in (a).

PdO decomposition and Pd oxidation cycles as a function of temperature, measured by heating of PdO or cooling of Pd^0 samples, in Figures 5 and 6, respectively. Data from the
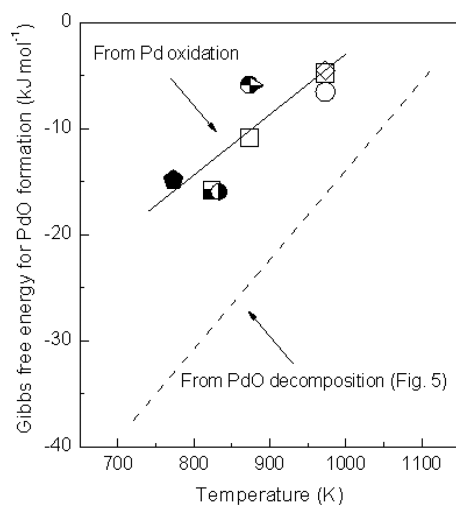

Figure 6. Gibbs free energies for PdO formation ($\Delta G^{\circ}_{Pd-PdO}$, per g-atom of Pd, eq 7), determined from Pd oxidation with O_2 (□: 8.8 nm mean Pd cluster diameter, ○: 2.2 nm mean Pd cluster diameter), Pd oxidation with CH_4-O_2 mixtures (◇: 8.8 nm mean Pd cluster diameter; 4.85 kPa CH_4), and those reported in the literature for Pd oxidation derived from cooling of metallic Pd from temperatures above that required for PdO decomposition (supported Pd clusters: ●,[39] half-filled right-pointing triangle,[42] ⬟,[4] ⬛,[5] ◐[4]). The line - - - denotes the Pd–PdO phase boundary calculated from linear regression of the PdO decomposition data from the literature and summarized in Figure 5, shown here for comparison.

oxidation of Pd by heating from low temperatures, as reported in the literature (e.g., oxidation occurred at ∼498 K during heating of 10 wt % Pd/Al$_2$O$_3$ from 293 to 1123 K),[40] were excluded in these comparisons because Pd oxidation at low temperatures is known to be limited by oxygen transport

bottlenecks and therefore inappropriate as a measure of the relevant free energies.

The Gibbs free energies derived from the PdO decomposition cycle (Figure 5) show the expected linear increase with temperature ($\Delta G^{\circ}_{Pd-PdO} = \Delta H^{\circ}_{Pd-PdO} - T\Delta S^{\circ}_{Pd-PdO}$, where $\Delta H^{\circ}_{Pd-PdO}$ and $\Delta S^{\circ}_{Pd-PdO}$ are the enthalpy and entropy changes for PdO formation from Pd, respectively, according to eq 7a; 500−1120 K), when compared among the various sources across the literature for small clusters,[4,5,39,42] bulk structures,[21,22] and single-crystal surfaces.[38,43] The linear trend was also found for the Gibbs free energies derived from cooling of metallic Pd (e.g., cooling from 1250 K in air)[42] to a temperature at which the incipient bulk oxidation occurs,[39,42,4,5] as depicted in Figure 5b. Gibbs free energies derived from decomposition and oxidation cycles (Figures 5 and 6) show similar linear dependencies but different absolute values, in contradiction to the purported thermodynamic origins of these previous data. Thus, one or both free energy values cannot reflect Pd−PdO thermodynamics.

The extreme temperature used for deriving the phase transition properties reported in the literature may cause Pd clusters to undergo extensive shape and structural transitions, driven not only by the bulk phase transition but also by the difference in the metal and oxide surface tensions and the extents of interaction between Pd (Pd^0 or PdO) and the underlying support. As temperature exceeds a critical value (up to 1143 K in air[17]), PdO clusters overcome the barriers for redispersion and begin to spread and wet the underlying substrate (Al$_2$O$_3$,[17] ZrO$_2$[8]) as an attempt to minimize their surface free energies. Such redispersion and spreading of PdO on the substrate lead a small portion of Pd atoms to form solid solution with the substrate. The PdO−substrate interactions increase the stability of these Pd atoms against decomposition and lead to more negative Gibbs free energies for PdO formation, which may contribute in part to the larger, more negative free energy values than expected, as previously reported and presented here in Figure 5. As these dispersed PdO domains, which interact strongly with the support, decompose, small Pd nuclei begin to form, migrate, and
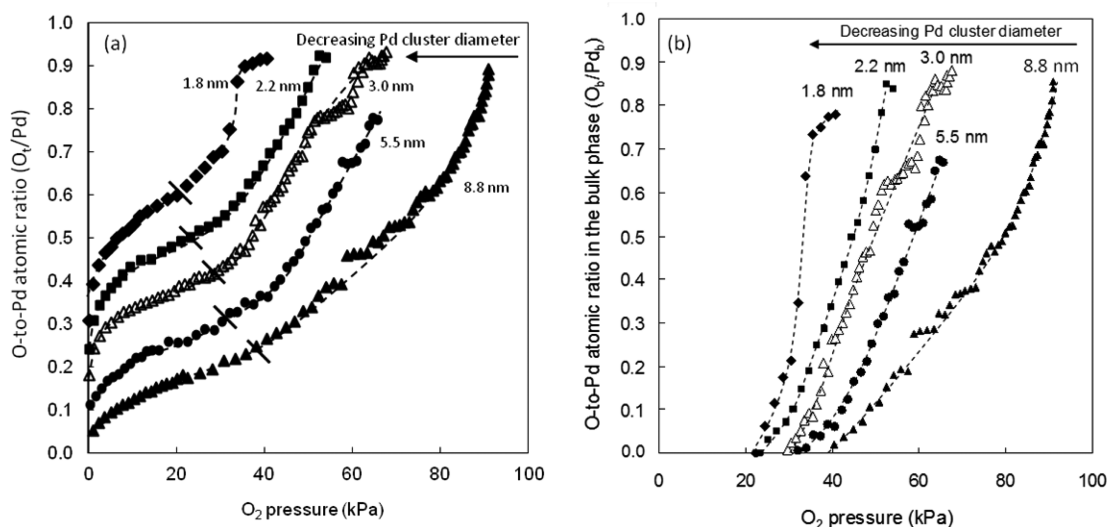
Figure 7. (a) Oxygen-to-Pd atomic ratios (O_t/Pd; $O_t = O_s^* + O_b$, Scheme 1) and (b) bulk oxygen-to-bulk Pd atomic ratios (O_b/Pd_b) in a series of Pd catalysts (0.6% wt. Pd/Al$_2$O$_3$ catalysts) with different mean cluster diameters of 1.8 nm (◆), 2.2 nm (■), 3.0 nm (△), 5.5 nm (●), and 8.8 nm (▲), plotted against equilibrium O$_2$ pressures at 973 K. The "−" denotes the O$_2$ pressures at which the oxygen uptakes increase above monolayer O* coverages. O_b/Pd_b ratios were obtained by subtracting the surface oxygen (O_s^*) and surface Pd (Pd_s) atoms from the total oxygen (O_t) and total Pd_t atoms [(O_b/Pd_b) = ($O_t − O_s^*$)/($Pd_t − Pd_s$); subscripts b, s, and t denote bulk, surface, and total, respectively; see details in Supporting Information, Section 2].

coalesce to larger Pd clusters because of their higher surface tension than PdO clusters and concomitantly higher interfacial tension between the Pd^0 clusters and the substrate than those for PdO.[17] In contrast, the cooling cycle (literature data in Figure 6) probes the oxidation of these large, agglomerated Pd clusters with weak metal substrate interactions as they were cooled to lower temperatures. The difference in surface and interfacial tensions for Pd and PdO may lead to the two sets of Gibbs free energy values for Pd oxidation and PdO decomposition. Reducible oxide supports such as CeO$_2$ may distort the structure and properties of Pd clusters and also become involved in O$_2$ activation or O* recombination, as evident from oxidation−reduction cycles that show much weaker temperature hysteresis when CeO$_2$ instead of Al$_2$O$_3$ are used as supports.[39] In contrast to these temperature cycling studies, Pd to PdO phase transitions (730−1200 K) attained complete reversibilities in an electrochemical cell prepared with intimate contact of Pd with the ceramic substrates and equipped with a Pt electrode, which promotes equilibration of oxygen by catalyzing the formation of O$^{2−}$ electrolyte from O$_2$(g) as a reactive oxidant for the oxidation of Pd in Pd−ceramic matrixes.[44] These electrochemical measurements on Pd−ceramic matrixes gave identical Gibbs free energies for both decomposition and oxidation cycles, and their values are similar to those derived from heating of PdO.

Our measurements were obtained from O$_2$ pressure cycles at a constant temperature (973 K) rather than with temperature cycles. The moderate temperature (973 K) used in our study eliminates the possibilities of Pd tethering between the wetted, dispersed solid oxide solution and the agglomerated metal clusters, thus removing the potential metal−support interactions and their corruptions in free energy measurements. Rate data confirm the complete reversal and path-independent nature of Pd−PdO interconversions with O$_2$, thus they represent the only definitive demonstration of the rigorous thermodynamic origins of these data and of the absence of any kinetic hurdles and secondary effects arising from metal−

support interactions. Our measurements provide compelling evidence that first-order CH$_4$ rate coefficients are single-valued functions of O$_2$ pressure (above 1.6 kPa CH$_4$) and show the same O$_2$ pressure dependence as O_t/Pd uptakes at 973 K (Figure 3). The coincidence of rate coefficients and oxygen uptake data and the rate coefficient values independent of path confirm that measured O_t/Pd uptakes rigorously reflect the thermodynamics of Pd−PdO phase transformations between Pd and PdO, with minimal contributions from the support. These data lead to the Gibbs free energies in Figure 6, which resemble those reported from the oxidation of Pd samples, presumably with minimal interactions with the support, as they were cooled from a temperature above PdO decomposition in the presence of O$_2$.[4,5,39,42] In contrast, free energies from PdO decomposition in Figure 5, including our results from the cycle of decreasing O$_2$ pressure (at 0 or <1.6 kPa CH$_4$), do not accurately reflect PdO−Pd thermodynamics because PdO redisperses on and interacts with the substrate as it is exposed to the high temperature required for its decomposition. On CeO$_2$ supports, oxidation−decomposition cycles show weaker hysteresis than on Al$_2$O$_3$,[39] suggesting less important transport restrictions. Oxygen transport restrictions were also minimized (and possibly removed) during CH$_4$−O$_2$ reactions on thin catalyst coatings (2 wt. % Pd/La$_2$O$_3$−Al$_2$O$_3$) in a small tubular reactor.[4] The Gibbs free energies for Pd oxidation, which were estimated based on the inflection points of rate coefficient profiles measured during temperature cyclings in CH$_4$−O$_2$ mixtures, remained essentially identical at approximately −15.9 kJ (mol$_{PdO}$)$^{−1}$ at 833 K for both Pd oxidation (cooling) and PdO decomposition (heating) (◐ in Figure 5 and ◑ in Figure 6);[4] these values appear to coincide and agree with the temperature-dependent free energy values (solid line in Figure 6) derived from Pd oxidation in the literature (◖,[39] half-filled right-pointing triangle,[42] ◆,[4] and □[5] in Figure 6) and from our data, which include those from Pd oxidation with O$_2$ and with CH$_4$−O$_2$ mixtures. The evidence provided here and the conclusions reached contradict previous assumptions[4,42,45]
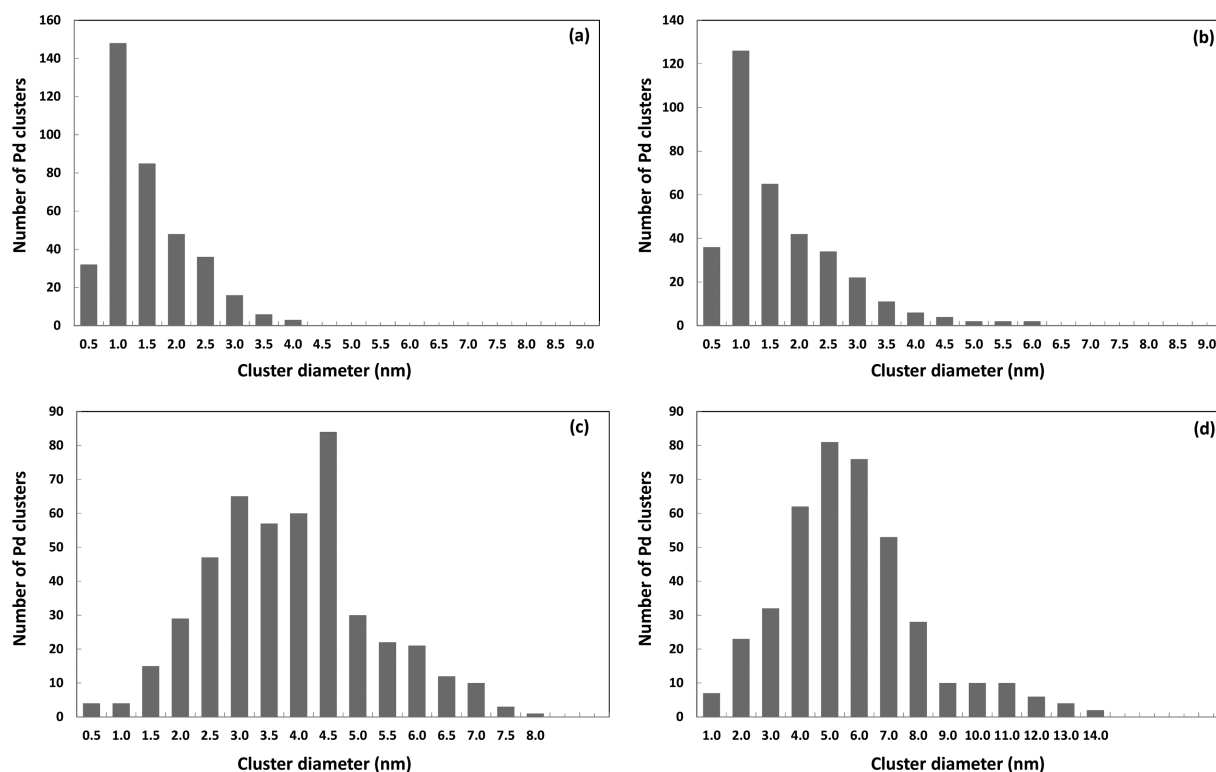
Figure 8. Cluster size distributions in 0.6% wt. Pd/Al$_2$O$_3$ samples with mean cluster diameters of 2.2 nm (a), 3.0 nm (b), 4.9 nm (c), and 8.0 nm (d), which correspond to the mean diameters of 2.2, 3.0, 5.5, and 8.8 nm, respectively, determined from oxygen chemisorption.

that PdO decomposition processes reflect the thermodynamics of this phase transition.[21,22]

3.4. Cluster Size Effects on Pd−PdO Thermodynamics. Small ensembles of atoms can exhibit chemical and physical properties that differ from their respective bulk phases. Heats of fusion[46] and melting temperatures[47−49] are lower for small clusters than their bulk structures. Here, we provide evidence for such effects of cluster size on Pd−PdO thermodynamics. These size effects are apparent from the effects of O$_2$ pressure on equilibrium O$_2$ uptakes (0.16−91 kPa O$_2$, 973 K) on 0.6% wt. Pd/Al$_2$O$_3$ samples that were treated to form Pd particles with mean diameters between 2.2 and 8.8 nm. Their sizes were determined from O$_2$ uptakes at pressures leading to surface O* saturation (without PdO formation) to be 2.2, 3.0, 5.5, and 8.8 nm, in reasonable agreement with surface-averaged cluster diameters from transmission electron microscopy (2.2, 3.0, 4.9, and 8.0 nm).

The equilibration among the bulk and surfaces of clusters and the contacting O$_2$(g) phase was confirmed for the largest clusters (8.8 nm) and assumed to remain so for smaller clusters (1.8−5.5 nm) with much shorter diffusion distances. Oxygen uptakes (O$_t$/Pd) on these samples correspond to monolayer O$_s$* coverages below a threshold O$_2$ pressure at which O$_s$*/Pd$_s$ equals unity, beyond which O$_s$* incipiently dissolutes into the cluster bulk (Supporting Information, Section 5, Figure S-6). This onset O$_2$ pressure (eq 6) increased with increasing mean cluster size (22 kPa for 1.8 nm; 35 kPa for 8.8 nm). This incipient "dissolution" phenomenon reflects the sequential conversion of Pd clusters in each sample into PdO, starting with the smallest clusters at the lowest O$_2$ pressure until the largest clusters become PdO. The O$_t$/Pd ratios at the plateau are slightly below stoichiometric values because a small fraction of the Pd atoms are dissolved in the Al$_2$O$_3$ support[18] and do

not undergo redox cycles. The increase in thermodynamic affinities toward oxidation for smaller than larger clusters is described next with a theoretical construction.

The amount of oxygen dissolved within a given cluster is expressed here as the oxygen-to-Pd atomic ratio in their bulk (O$_b$/Pd$_b$, subscript b denotes bulk), excluding O$_s$* and the Pd atoms at surfaces (Pd$_s$); the O$_b$/Pd$_b$ determination is illustrated in Supporting Information, Section 2. These bulk O$_b$/Pd$_b$ ratios (Figure 7) start to increase gradually above an onset O$_2$ pressure (e.g., 22 kPa O$_2$ for 1.8 nm Pd clusters) to values near those expected for PdO (O$_b$/Pd$_b$ = 1, measured values >0.7) over a broad O$_2$ pressure range. The onset O$_2$ pressure increases with increasing cluster diameter, consistent with the more favorable oxidation thermodynamics for the clusters with the smallest mean size. Pd−PdO transitions do not occur sharply as O$_2$ pressures increase (Figure 7) and thus do not behave as expected from the Gibbs phase rule. The gradual increase in O$_b$/Pd$_b$ ratios reflects the cumulative O$_2$ uptakes from clusters distributed in size and thermodynamic properties. Next, we demonstrate that smaller Pd clusters convert to PdO at lower O$_2$ pressures because of their more negative Gibbs free energy for PdO formation (ΔG°_{Pd-PdO} in eq 7b) and higher tendencies toward bulk oxidation than larger clusters.

The cluster size distributions (Figure 8) for samples with mean diameters of 2.2, 3.0, 4.9, and 8.0 nm are used next to determine the variation in Gibbs free energies for Pd−PdO transformations (ΔG°_{Pd-PdO}, eqs 7a and 7b) with cluster diameter. First, clusters in each sample are grouped within "size bins" (e.g., 0.5−1.0 nm, 1.1−1.5 nm, ... for 2.2, 3.0, and 4.9 nm mean diameters and 0−1.0 nm, 1.1−2.0 nm, etc. ... for 8.0 nm mean diameter, in Figure 8). Measured O$_2$ uptakes for each sample (O$_b$/Pd$_b$, Figure 7) are then used to sequentially titrate the bulk of the clusters within each bin with O atoms, starting
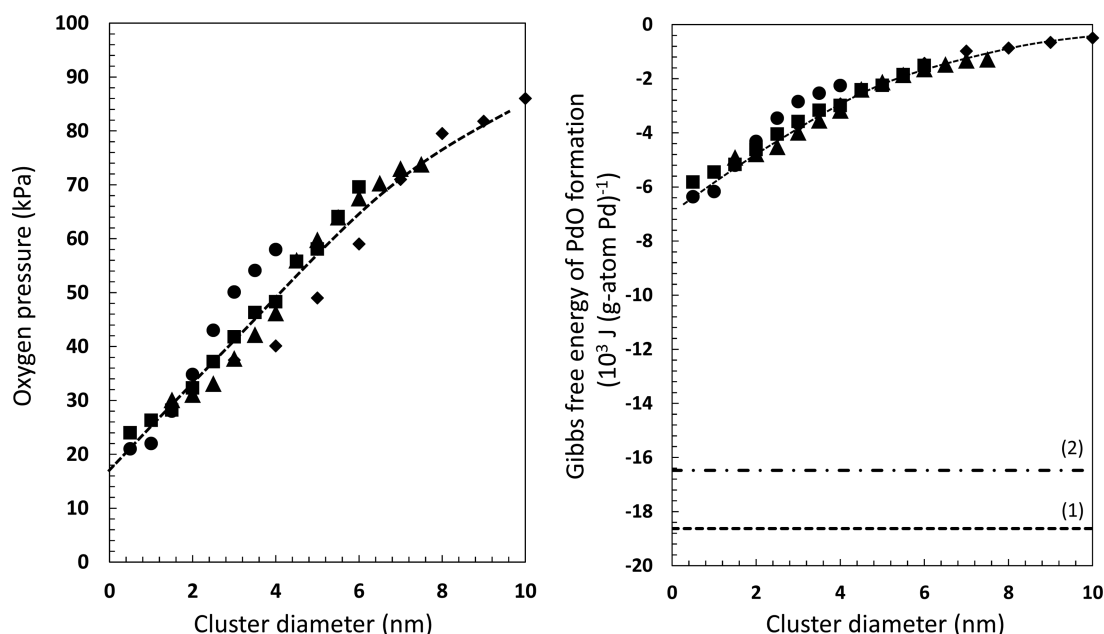
Figure 9. (a) O_2 pressure required for incipient phase transition for each cluster diameter range and (b) Gibbs free energies for PdO formation ($\Delta G^{\circ}_{Pd-PdO}$, per g-atom of Pd, eq 7) at 973 K as a function of Pd cluster diameter in Pd/Al$_2$O$_3$ samples with average cluster diameters of 2.2 nm (●), 3.0 nm (■), 5.5 nm (▲), and 8.8 nm (♦). The data from Wang and Huebner (labeled (1))[54] and Nell and O'Neill (labeled (2))[44] at 973 K are included for comparison.

from the smallest clusters as O_2 pressure increases (illustrative examples in Supporting Information, Section 6). The number of atoms in the clusters within a given bin is calculated as that for cubooctahedral fcc clusters. All clusters in a bin are assumed to form PdO at one given O_2 pressure, corresponding to its free energy for Pd oxidation and as required by the Gibbs phase rule.

The onset O_2 pressures and the respective free energies ($\Delta G^{\circ}_{Pd-PdO}$, 973 K, 1 bar) are shown in Figures 9a and 9b, respectively, as a function of cluster diameter for each sample. The oxidation thermodynamics of Pd metal clusters depend on their size, in a manner that reflects only the size of the clusters within a bin, irrespective of the specific sample from which such clusters are chosen. All samples show overlapping free energies, consistent with Pd–PdO phase transitions that are more favorable (more negative Gibbs free energy; transitions at lower O_2 pressures) for smaller clusters. For example, Gibbs free energies ($\Delta G^{\circ}_{Pd-PdO}$, per g-atom of Pd, 1 bar, 973 K) are more negative for 1 nm clusters $[-6 \text{ kJ } (\text{mol}_{PdO})^{-1}]$ than for bulk PdO $[-0.5 \text{ kJ } (\text{mol}_{PdO})^{-1}]$ (Figure 9b). These smaller clusters in their metallic state are expected to bind chemisorbed oxygen more strongly at their surfaces than larger clusters because of their lower surface coordination, as confirmed from the higher temperatures required to desorb chemisorbed O* atoms from Pd clusters (750 K for 1.6 nm vs 700 K for 9.1 nm clusters).[50] The stronger binding to O* and the more negative free energies for PdO formation (Figure 9b) found in these smaller clusters than the bulk structures appear to follow the linear correlation between the O* binding strengths $[Q_{O*-Pd} = (-\Delta H_{O*-Pd})$ for oxygen dissociation, Step 1 of Scheme 2] and heats of bulk oxide formation $[Q_{Pd-PdO} = (-\Delta H^{\circ}_{Pd-PdO}) = -(\Delta G^{\circ}_{Pd-PdO} + T\Delta S^{\circ}_{Pd-PdO})]$, established previously by varying the metal identity across bulk transition metals.[51,52] The instabilities of small metallic clusters have also been shown from an increase in the heat of cluster adhesion on oxide surfaces [e.g., for 1−4 nm Pb on MgO(100)] to values much

larger than predicted with the Gibbs−Thomson model by microcalorimetry.[53] These enthalpic instabilities in small clusters lead, in turn, to their greater tendency for bulk oxidation (Figure 9). Even though the clusters in this study are relatively small, their Gibbs free energies for PdO formation $[\Delta G^{\circ}_{Pd-PdO}$ values range from −6.5 kJ $(\text{mol}_{PdO})^{-1}$ to −1.4 kJ $(\text{mol}_{PdO})^{-1}$ for 0.5 to 10 nm cluster diameters, Figure 9b] remain much less negative than previously reported data [e.g., −18.6 kJ $(\text{mol}_{PdO})^{-1}$ (polycrystalline sample),[54] −16.5 kJ $(\text{mol}_{PdO})^{-1}$ (polycrystalline sample),[44] and −14 kJ $(\text{mol}_{PdO})^{-1}$ (from regression of the data in Figure 5a); all data were interpolated/extrapolated to 973 K] derived from PdO decomposition, which appear to reflect either kinetic hurdles or strong metal−support interactions instead of true Pd−PdO thermodynamics (Section 3.3).

3.5. Effects of the Bulk Chemical State of Pd Clusters on C−H Bond Activation Turnover Rates. The effects of oxygen content and of the Pd−PdO transformation on C−H activation rates at 973 K for Pd/Al$_2$O$_3$ (8.8 nm mean cluster diameter) are shown in Figure 10. In this figure, the (total) oxygen content includes O atoms at surfaces and (if any) in the cluster bulk. C−H bond activation rate coefficients (k_{CH_4}, eq 5; 973 K) remained nearly constant [0.73 mol CH$_4$ (g-atom Pd$_{surface}$ kPa s)$^{-1}$; 973 K] with increasing O content at O$_t$/Pd ratios less than 0.11, which reflect the predominant presence of O atoms at Pd cluster surfaces. The bulk of small clusters, present as minority species in this sample (Figure 8d), may convert to PdO at these conditions, leading to these low O$_t$/Pd ratios, but their reactivity remains low because of the strong Pd−O bonds and less reactive O^{2-} ions toward the H abstraction step, as shown previously from size effects on CH$_4$ turnover rates.[8] Chemisorbed oxygen atoms (O$_s$*) present at saturation coverages on Pd^0 clusters activate C−H bonds via homolytic processes in which one O$_s$* atom abstracts a H atom from CH$_4$ and forms an adsorbed O−H bond, while another O$_s$* interacts weakly with the radical-like CH$_3$ group at the
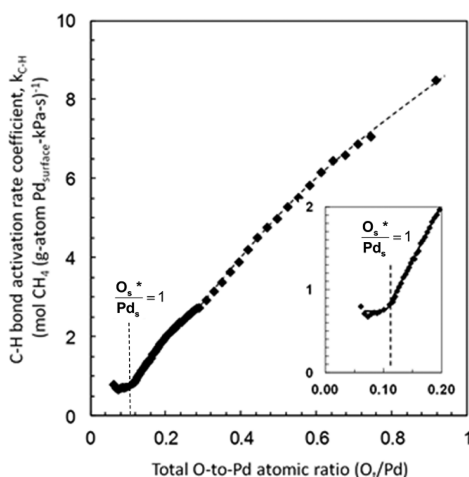
Figure 10. Effects of total oxygen-to-Pd atomic ratio (O_t/Pd) on C−H bond activation rate coefficients for CH_4−O_2 reactions on Pd clusters (0.6% wt. Pd/Al_2O_3 catalyst; 8.8 nm mean Pd cluster diameter) at 973 K. Inset: Enlarged plot for the low total oxygen-to-Pd atomic (O_t/Pd) ratio region between 0 and 0.20. CH_4−O_2 rates were measured at 6.51×10^8 cm^3 (s mol Pd$_{surface}$)$^{-1}$.

transition state,[3] as also reported for CH_4[13,55] and C_2H_6[27] on Pt cluster surfaces saturated with O_s*. As O_t/Pd ratios increase above 0.11, a larger fraction of the O_s*-saturated Pd clusters transforms to PdO, starting with the smallest clusters, as described in Section 3.4. As O_t/Pd ratios increase to values above monolayer coverages, the rate coefficients increase monotonically with O_t/Pd ratio over the entire O_t/Pd range (0.11−0.92, Figure 10), until both rates and O contents reach the asymptotic values corresponding to PdO. These monotonic trends of rate coefficients with O_t/Pd ratios (Figure 10) indicate that C−H bond activation remains as the kinetically relevant step throughout the bulk phase transition but occurs more effectively as bulk oxidation exposes Pd^{2+} atoms and Pd^{2+}−O^{2-} site pairs at surfaces of large clusters. The rate coefficient increases near linearly with the oxygen contents but deviates to slightly lower than the linear trend at higher oxygen contents (>0.68 O_t/Pd ratio). The apparent lower rate coefficients may reflect the oxidation of the larger Pd clusters, which contain fewer Pd^{2+}−O^{2-} sites (per bulk Pd atom) than the smaller clusters. Such effects are offset by the higher C−H bond activation rate coefficients (per site) on these larger clusters, as weakly bound and more reactive oxygen species are prevalent for the H abstraction step. These effects of site numbers and structure sensitivities may compensate each other and result in the near linear relation between the rate coefficients and oxygen contents. The Pd^{2+}−O^{2-} pairs prevalent on the PdO cleave the C−H bonds in CH_4 more effectively than the O* pairs on O*-saturated Pd surfaces and do so via σ-bond metathesis pathways through stable four-center transition states ($HC_3{}^{\delta-}$−Pd^{2+}−O^{2-}−$H^{\delta+}$)‡ with strong $HC_3{}^{\delta-}$−Pd^{2+}, Pd^{2+}−$H^{\delta+}$, O^{2-}−$H^{\delta+}$, and $HC_3{}^{\delta-}$−$H^{\delta+}$ inter-actions;[13,16,27] such structures are reminiscent of those involved in C−H activation by organometallic complexes [e.g., W-$(OH)_2(—NH)$[56]], as discussed in recent studies.[3]

4. CONCLUSIONS

Thermodynamics of nanometer-sized Pd clusters and their kinetic consequences for methane oxidation were probed after eliminating corruptions caused by oxygen transports among the gas phase, cluster surfaces, and cluster bulk and by the inherent cluster size distributions within a catalyst sample. Oxygen equilibration was rigorously confirmed from (1) coincided profiles of C−H activation rate coefficient and mean oxygen content (and therefore chemical state) of Pd with increasing oxygen chemical potential and (2) C−H activation rate coefficients as a single-valued function of oxygen chemical potential, irrespective of their path and treatment history. Chemical equilibration of oxygen was attained during Pd oxidation, irrespective of CH_4 pressures. In contrast, the oxygen equilibrium was not attained during PdO decomposition because nucleation of the Pd atom ensembles on PdO surfaces requires consecutive removal of lattice oxygen atoms near oxygen vacancies in steps that are kinetically prohibitive without CH_4. Such kinetic restrictions are removed by CH_4 (above a critical CH_4 pressure), as CH_4 oxidation catalysis converts the lattice oxygen atoms into surface hydroxyl intermediates, which recombine and desorb as water, in an energetically favorable path. PdO decomposition in O_2 without admixed CH_4 is either kinetically limited or influenced by strong metal−support interactions, yet this step has been used widely across the literature to establish the Pd−PdO phase boundary and the heat of PdO formation, despite the fact that complete reversibility and oxygen equilibration have not been demonstrated. A theoretical construction accounting for the inherent size variance of Pd clusters within a sample is used to demonstrate the strong effects of cluster diameter on their thermodynamic tendency toward bulk oxidation. The Gibbs free energy for PdO formation is more negative, and the associated thermodynamic tendency for incipient bulk oxidation is higher for smaller Pd clusters than their large structures. C−H bond activation rate constants increase monotonically with the mean oxygen contents, as a portion of Pd clusters undergoes incipient phase transition to PdO and the active sites on these clusters concomitantly convert from O* adatom pairs to O^{2-} and Pd^{2+} ion pairs. The O^{2-} and Pd^{2+} ion pairs assist in C−H bond activation via σ-bond metathesis pathways and stabilize the C−H bond activation transition state to a larger extent than the O* adatom pairs through four-center ($HC_3{}^{\delta-}$−Pd^{2+}−O^{2-}−$H^{\delta+}$)‡ transition states with stronger Pd^{2+}−$CH_3{}^{\delta-}$, Pd^{2+}−$H^{\delta+}$, and $HC_3{}^{\delta-}$−$H^{\delta+}$ interactions.

■ ASSOCIATED CONTENT

Ⓢ Supporting Information

The Supporting Information is available free of charge on the ACS Publications website at DOI: 10.1021/acs.jpcc.5b06677.

> Time-dependent oxygen contents for 8.8 nm Pd clusters (0.6% wt. Pd/Al_2O_3 catalysts); bulk oxygen-to-bulk Pd atomic ratios; comparison of the O_2 pressures required for PdO decomposition and Pd oxidation; Gibbs free energies for PdO formation; oxygen-to-Pd atomic ratios; a theoretical construction for decoupling cluster size distribution effects from the cluster diameter effects on the bulk phase transition of Pd clusters (PDF)

■ AUTHOR INFORMATION

Corresponding Author

*E-mail: iglesia@berkeley.edu. Phone: (925) 323-5559.

Present Address

†Department of Chemical Engineering and Applied Chemistry, University of Toronto, Toronto, ON M5S 3E5, Canada.

■ REFERENCES

(1) Zhu, G. H.; Han, J. Y.; Zernlyanov, D. Y.; Ribeiro, F. H. Temperature Dependence of the Kinetics for the Complete Oxidation of Methane on Palladium and Palladium Oxide. *J. Phys. Chem. B* **2005**, *109*, 2331−2337.

(2) Lyubovsky, M.; Pfefferle, L. Complete Methane Oxidation over Pd Catalyst Supported on Alpha-Alumina. Influence of Temperature and Oxygen Pressure on the Catalyst Activity. *Catal. Today* **1999**, *47*, 29−44.

(3) Chin, Y. H.; Buda, C.; Neurock, M.; Iglesia, E. Consequences of Metal-Oxide Interconversion for C-H Bond Activation During CH_4 Reactions on Pd Catalysts. *J. Am. Chem. Soc.* **2013**, *135*, 15425−15442.

(4) McCarty, J. G. Kinetics of PdO Combustion Catalysis. *Catal. Today* **1995**, *26*, 283−293.

(5) Baylet, A.; Marecot, P.; Duprez, D.; Castellazzi, P.; Groppi, G.; Forzatti, P. In Situ Raman and In Situ XRD Analysis of PdO Reduction and Pd Degrees Oxidation Supported on Gamma-Al_2O_3 Catalyst under Different Atmospheres. *Phys. Chem. Chem. Phys.* **2011**, *13*, 4607−4613.

(6) Salomonsson, P.; Johansson, S.; Kasemo, B. Methane Oxidation over PdO_x-on the Mechanism for the Hysteresis in Activity and Oxygen-Content. *Catal. Lett.* **1995**, *33*, 1−13.

(7) Garbowski, E.; Feumijantou, C.; Mouaddib, N.; Primet, M. Catalytic Combustion of Methane over Palladium Supported on Alumina Catalysts: Evidence for Reconstruction of Particles. *Appl. Catal., A* **1994**, *109*, 277−291.

(8) Fujimoto, K.; Ribeiro, F. H.; Avalos-Borja, M.; Iglesia, E. Structure and Reactivity of PdO_x/ZrO_2 Catalysts for Methane Oxidation at Low Temperatures. *J. Catal.* **1998**, *179*, 431−442.

(9) Farrauto, R. J.; Hobson, M. C.; Kennelly, T.; Waterman, E. M. Catalytic Chemistry of Supported Palladium for Combustion of Methane. *Appl. Catal., A* **1992**, *81*, 227−237.

(10) Su, S. C.; Carstens, J. N.; Bell, A. T. A Study of the Dynamics of Pd Oxidation and PdO Reduction by H_2 and CH_4. *J. Catal.* **1998**, *176*, 125−135.

(11) Chen, J. J.; Ruckenstein, E. Role of Interfacial Phenomena in the Behavior of Alumina-Supported Palladium Crystallites in Oxygen. *J. Phys. Chem.* **1981**, *85*, 1606−1612.

(12) Hicks, R. F.; Qi, H. H.; Young, M. L.; Lee, R. G. Effect of Catalyst Structure on Methane Oxidation over Palladium on Alumina. *J. Catal.* **1990**, *122*, 295−306.

(13) Chin, Y. H.; Buda, C.; Neurock, M.; Iglesia, E. Reactivity of Chemisorbed Oxygen Atoms and Their Catalytic Consequences During CH_4-O_2 Catalysis on Supported Pt Clusters. *J. Am. Chem. Soc.* **2011**, *133*, 15958−15978.

(14) Chou, T. Y.; Hwang, C. P.; Yeh, C. T. Graphic Determination of Kinetic Parameters in Temperature-Programmed Desorption of Oxygen from Alumina-Supported PdO. *J. Therm. Anal.* **1996**, *46*, 305−315.

(15) Haynes, W. M. *CRC Handbook of Chemistry and Physics: A Ready-Reference Book of Chemical and Physical Data*, 93rd ed.; CRC Press: Boca Raton, Fl; London, 2012; pp 4−79.

(16) Chin, Y. H.; Iglesia, E. Elementary Steps, the Role of Chemisorbed Oxygen, and the Effects of Cluster Size in Catalytic CH_4-O_2 Reactions on Palladium. *J. Phys. Chem. C* **2011**, *115*, 17845−17855.

(17) Ruckenstein, E.; Chen, J. J. Spreading and Surface-Tension Gradient Driven Phenomena During Heating of Alumina-Supported Palladium Crystallites in Oxygen. *J. Catal.* **1981**, *70*, 233−236.

(18) Castellazzi, P.; Groppi, G.; Forzatti, P.; Baylet, A.; Marecot, P.; Duprez, D. Role of Pd Loading and Dispersion on Redox Behaviour and CH_4 Combustion Activity of Al_2O_3 Supported Catalysts. *Catal. Today* **2010**, *155*, 18−26.

(19) Lu, Z. S.; Yang, Z. X.; He, B. L.; Castleton, C.; Hermansson, K. Cu-Doped Ceria: Oxygen Vacancy Formation Made Easy. *Chem. Phys. Lett.* **2011**, *510*, 60−66.

(20) Han, J. Y.; Zemlyanov, D. Y.; Ribeiro, F. H. Interaction of O_2 with Pd Single Crystals in the Range 1−150 Torr: Oxygen Dissolution and Reaction. *Surf. Sci.* **2006**, *600*, 2752−2761.

(21) Zhang, H.; Gromek, J.; Fernando, G. W.; Boorse, S.; Marcus, H. L. PdO/Pd System Equilibrium Phase Diagram under a Gas Mixture of Oxygen and Nitrogen. *J. Phase Equilib.* **2002**, *23*, 246−248.

(22) Bayer, G.; Wiedemann, H. G. Formation, Dissociation and Expansion Behavior of Platinum Group Metal-Oxides (PdO, RuO_2, IrO_2). *Thermochim. Acta* **1975**, *11*, 79−88.

(23) Bell, W. E.; Inyard, R. E.; Tagami, M. Dissociation of Palladium Oxide. *J. Phys. Chem.* **1966**, *70*, 3735−3736.

(24) Iglesia, E.; Spivey, J. J.; Fleisch, T. H. *Natural Gas Conversion VI: Proceedings of the 6th Natural Gas Conversion Symposium, June 17−22, 2001, Alaska, USA*; Elsevier: Amsterdam; New York, 2001; p xiii, 561 p.

(25) Groppi, G.; Artioli, G.; Cristiani, C.; Lietti, L.; Forzatti, P. Decomposition/reformation Process in CH_4 Combustion Activity of PdO Over Alumina Supported Catalysts for Gas Turbine Applications. *Stud. Surf. Sci. Catal.* **2001**, *136*, 345−350.

(26) Boudart, M. Thermodynamic and Kinetic Coupling of Chain and Catalytic Reactions. *J. Phys. Chem.* **1983**, *87*, 2786−2789.

(27) Garcia-Dieguez, M.; Chin, Y. H.; Iglesia, E. Catalytic Reactions of Dioxygen with Ethane and Methane on Platinum Clusters: Mechanistic Connections, Site Requirements, and Consequences of Chemisorbed Oxygen. *J. Catal.* **2012**, *285*, 260−272.

(28) Weiss, B. M.; Artioli, N.; Iglesia, E. Catalytic NO Oxidation Pathways and Redox Cycles on Dispersed Oxides of Rhodium and Cobalt. *ChemCatChem* **2012**, *4*, 1397−1404.

(29) Weiss, B. M.; Iglesia, E. Mechanism and Site Requirements for NO Oxidation on Pd Catalysts. *J. Catal.* **2010**, *272*, 74−81.

(30) Weiss, B. M.; Iglesia, E. NO Oxidation Catalysis on Pt Clusters: Elementary Steps, Structural Requirements, and Synergistic Effects of NO_2 Adsorption Sites. *J. Phys. Chem. C* **2009**, *113*, 13331−13340.

(31) Temkin, M.; Pyzhev, V. Kinetics of Ammonia Synthesis on Promoted Iron Catalysts. *Acta Physicochim. URSS* **1940**, *12*, 327−356.

(32) Iglesia, E.; Baumgartner, J. E.; Price, G. L. Kinetic Coupling and Hydrogen Surface Fugacities in Heterogeneous Catalysts: 1. Alkane Reactions on Te/NaX, H-ZSM5, and Ga/H-ZSM5. *J. Catal.* **1992**, *134*, 549−571.

(33) Yu, S. Y.; Biscardi, J. A.; Iglesia, E. Kinetic Relevance of Hydrogen Desorption Steps and Virtual Pressures on Catalytic Surfaces During Reactions of Light Alkanes. *J. Phys. Chem. B* **2002**, *106*, 9642−9648.

(34) Guo, X. C.; Madix, R. J. Oxygen-Activated Combustion of Alkenes on the Pd(100) Surface. *J. Am. Chem. Soc.* **1995**, *117*, 5523−5530.

(35) Todorova, M.; Reuter, K.; Scheffler, M. Oxygen Overlayers on Pd(111) Studied by Density Functional Theory. *J. Phys. Chem. B* **2004**, *108*, 14477−14483.

(36) Weaver, J. F.; Hinojosa, J. A.; Hakanoglu, C.; Antony, A.; Hawkins, J. M.; Asthagiri, A. Precursor-Mediated Dissociation of N-Butane on a PdO(101) Thin Film. *Catal. Today* **2011**, *160*, 213−227.

(37) Zheng, G.; Altman, E. I. The Oxidation of Pd(111). *Surf. Sci.* **2000**, *462*, 151−168.

(38) Gabasch, H.; Unterberger, W.; Hayek, K.; Klötzer, B.; Kleimenov, E.; Teschner, D.; Zafeiratos, S.; Hävecker, M.; Knop-Gericke, A.; Schlögl, R.; Han, J.; Ribeiro, F. H.; Aszalos-Kiss, B.; Curtin, T.; Zemlyanov, D. In Situ XPS Study of Pd(111) Oxidation at Elevated Pressure, Part 2: Palladium Oxidation in the 10^{-1} mbar Range. *Surf. Sci.* **2006**, *600*, 2980−2989.

(39) Farrauto, R. J.; Lampert, J. K.; Hobson, M. C.; Waterman, E. M. Thermal-Decomposition and Reformation of PdO Catalyst-Support Effects. *Appl. Catal., B* **1995**, *6*, 263−270.

(40) Hoost, T. E.; Otto, K. Temperature-Programmed Study of the Oxidation of Palladium Alumina Catalysts and Their Lanthanum Modification. *Appl. Catal., A* **1992**, *92*, 39−58.

(41) Dushman, S. *Scientific Foundations of Vacuum Technique*, 2nd ed.; John Wiley & Sons: New York, 1962; p 748.

(42) Datye, A. K.; Bravo, J.; Nelson, T. R.; Atanasova, P.; Lyubovsky, M.; Pfefferle, L. Catalyst Microstructure and Methane Oxidation Reactivity During the Pd<- > PdO Transformation on Alumina Supports. *Appl. Catal., A* **2000**, *198*, 179−196.

(43) Zheng, G.; Altman, E. I. The Oxidation Mechanism of Pd(100). *Surf. Sci.* **2002**, *504*, 253−270.

(44) Nell, J.; O'Neill, H. S. Gibbs Free Energy of Formation and Heat Capacity of PdO: A New Calibration of the Pd-PdO Buffer to High Temperatures and Pressures. *Geochim. Cosmochim. Acta* **1996**, *60*, 2487−2493.

(45) Gabasch, H.; Hayek, K.; Klötzer, B.; Unterberger, W.; Kleimenov, E.; Teschner, D.; Zafeiratos, S.; Hävecker, M.; Knop-Gericke, A.; Schlögl, R.; Aszalos-Kiss, B.; Zemlyanov, D. Methane Oxidation on Pd(111): In Situ XPS Identification of Active Phase. *J. Phys. Chem. C* **2007**, *111*, 7957−7962.

(46) Bachels, T.; Guntherodt, H. J.; Schafer, R. Melting of Isolated Tin Nanoparticles. *Phys. Rev. Lett.* **2000**, *85*, 1250−1253.

(47) Li, T. X.; Ji, Y. L.; Yu, S. W.; Wang, G. H. Melting Properties of Noble Metal Clusters. *Solid State Commun.* **2000**, *116*, 547−550.

(48) Cleveland, C. L.; Luedtke, W. D.; Landman, U. Melting of Gold Clusters. *Phys. Rev. B: Condens. Matter Mater. Phys.* **1999**, *60*, 5065−5077.

(49) Roduner, E. Size Matters: Why Nanomaterials Are Different. *Chem. Soc. Rev.* **2006**, *35*, 583−592.

(50) Putna, E. S.; Vohs, J. M.; Gorte, R. J. Oxygen Desorption from Alpha-Al_2O_3(0001) Supported Rh, Pt and Pd Particles. *Surf. Sci.* **1997**, *391*, L1178−L1182.

(51) Brennan, D.; Hayward, D. O.; Trapnell, B. M. W. The Calorimetric Determination of the Heats of Adsorption of Oxygen on Evaporated Metal Films. *Proc. R. Soc. London, Ser. A* **1960**, *256*, 81−105.

(52) Tanaka, K. I.; Tamaru, K. A General Rule in Chemisorption of Gases on Metals. *J. Catal.* **1963**, *2*, 366−370.

(53) Campbell, C. T.; Parker, S. C.; Starr, D. E. The Effect of Size-Dependent Nanoparticle Energetics on Catalyst Sintering. *Science* **2002**, *298*, 811−814.

(54) Wang, S. F.; Huebner, W. Thermodynamic Modeling of Equilibrium Subsolidus Phase Relations in the Ag-Pd-O_2 System. *J. Am. Ceram. Soc.* **1991**, *74*, 1349−1359.

(55) Chin, Y. H.; Buda, C.; Neurock, M.; Iglesia, E. Selectivity of Chemisorbed Oxygen in C-H Bond Activation and CO Oxidation and Kinetic Consequences for CH_4-O_2 Catalysis on Pt and Rh Clusters. *J. Catal.* **2011**, *283*, 10−24.

(56) Cundari, T. R. Calculation of a Methane C-H Oxidative Addition Trajectory- Comparison to Experiment and Methane Activation by High-Valent Complexes. *J. Am. Chem. Soc.* **1994**, *116*, 340−347.